

Microemulsions in the driven Widom-Rowlinson lattice gas

Maxim O. Lavrentovich*

Department of Physics & Astronomy, University of Tennessee, Knoxville, Tennessee 37996, USA

Ronald Dickman†

Departamento de Física and National Institute of Science and Technology for Complex Systems, ICEX, Universidade Federal de Minas Gerais, C. P. 702, 30123-970 Belo Horizonte, Minas Gerais, Brazil

R. K. P. Zia‡

Center for Soft Matter and Biological Physics, Department of Physics, Virginia Polytechnic Institute & State University, Blacksburg, Virginia 24061, USA and Physics Department, University of Houston, Houston, Texas 77204, USA

An investigation of the two-dimensional Widom-Rowlinson lattice gas under an applied drive uncovered a remarkable non-equilibrium steady state in which uniform stripes (reminiscent of an equilibrium lamellar phase) form perpendicular to the drive direction [R. Dickman and R. K. P. Zia, *Phys. Rev. E* **97**, 062126 (2018)]. Here we study this model at low particle densities in two and three dimensions, where we find a disordered phase with a characteristic length scale (a “microemulsion”) along the drive direction. We develop a continuum theory of this disordered phase to derive a coarse-grained field-theoretic action for the non-equilibrium dynamics. The action has the form of two coupled driven diffusive systems with *different* characteristic velocities, generated by an interplay between the particle repulsion and the drive. We then show how fluctuation corrections in the field theory may generate the characteristic features of the microemulsion phase, including a peak in the static structure factor corresponding to the characteristic length scale. This work lays the foundation for understanding the stripe phenomenon more generally.

I. INTRODUCTION AND BACKGROUND

Modulated or spatially-patterned phases abound in and out of equilibrium: Block copolymers, magnetic thin films, type-I superconductor films in applied magnetic fields, cholesteric liquid crystals [1], and lipid mixtures may all exhibit thermodynamically stable, patterned equilibrium phases [2]. On the other hand, driven granular systems [3], Rayleigh-Bénard convection rolls [4], and other out-of-equilibrium systems exhibit spatially-modulated, dynamical steady states [5], as well. In these systems, when an equilibrium, free-energy-based treatment is appropriate, one may often define a coarse-grained scalar order parameter $\psi(\mathbf{r})$ which, in the ordered phase, has some spatial modulation with a characteristic wavenumber $q^* = 2\pi/\lambda^*$ describing the pattern size λ^* . A common ordered phase consists of stripes (or slabs, in 3D) with $\psi(\mathbf{r}) \propto \cos(q^*x)$ for describing a structure periodic in some $\hat{\mathbf{x}}$ direction.

In the disordered phase, with $\langle \psi \rangle = 0$ on average, the characteristic pattern size may also show up as a peak in the static structure factor at q^* . Such a peak is observed in scattering intensity distributions of oil-and-water mixtures, which may be treated with a phenomenological free energy of the kind considered here [6]. We therefore refer to the “structured” disordered phase as a microemulsion. Such a phase is character-

ized by clustering at a particular length scale λ^* , but without any long-range, ordered patterning. Such phases may contain droplets or have a bicontinuous, disordered structure. The presence of a characteristic $q^* > 0$ in the disordered phase also strongly modifies the phase behavior, as the thermal fluctuations of the order parameter ψ occur predominantly in a non-zero momentum “shell” $|\mathbf{q}| = q^*$.

For the systems admitting an equilibrium treatment, the origin of the special scale q^* may come from some competing interactions, such as a coupling of a lipid membrane composition to the membrane curvature [7] or be set by particular boundary conditions [4]. Once the scale q^* has been identified, such systems near the pattern-formation transition are described by a phenomenological, coarse-grained free energy, first analyzed by Brazovskii and coworkers [8, 9]. In this work, we explore a system where the scale q^* develops unexpectedly and no coarse-grained free energy is *a priori* available due to the explicitly out-of-equilibrium state of the system: The patterns develop in a phase-separating binary mixture of particles with purely repulsive interactions under an applied drive [10]. We will show that the origin of q^* is subtle in this case, and results from an interplay between the repulsive interactions and the applied drive.

Strongly-driven physical systems exhibit a range of out-of-equilibrium, pattern-forming phenomena. For example, laning or striped behavior is known to occur in a wide range of systems, including vibrated granular mixtures with varying friction coefficients [11], driven polymer blends [12], and binary plasmas [13]. In most of these systems, the stripes form parallel to the drive di-

* lavrentm@gmail.com

† dickman@fisica.ufmg.br

‡ rkpzia@vt.edu

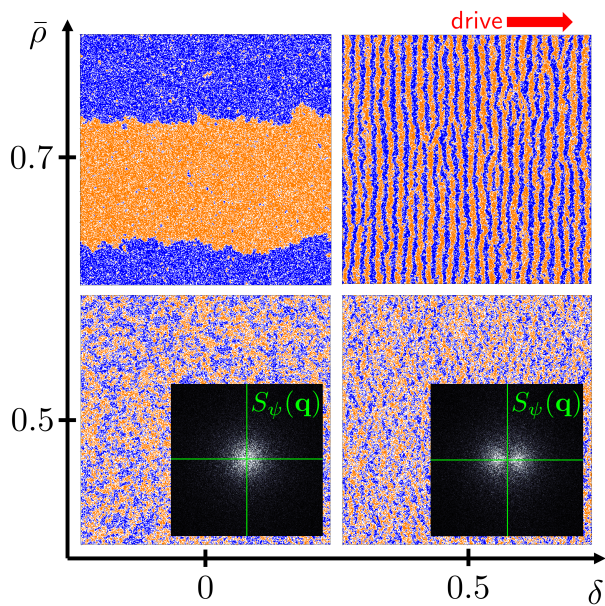


FIG. 1. Snapshots of steady states of the driven Widom-Rowlinson lattice gas (DWRLG) for a $L \times L$ system with $L = 400$ with equal mixtures of blue and orange particles. At high densities ($\bar{\rho} = 0.7$), the mixture phase separates either completely without a drive ($\delta = 0$) or into uniform stripes with a drive ($\delta = 0.5$). At lower densities ($\bar{\rho} = 0.5$), the particles remain mixed. In the presence of a drive, in the direction given by the red arrow, the disordered phase has a characteristic length scale as can be observed from the static structure factors $S_\psi(\mathbf{q})$ (the insets). Note that the $\delta = 0$ case has a single peak at the origin, while the $\delta = 0.5$ case has two maxima away from the origin along the drive direction.

rection. Moreover, the size of the stripes is typically set by either the microscopic constituents of the model, or by the system size [14]. Otherwise, non-trivial spatial modulations appear to emerge in systems with long-range particle-hole exchanges [15]. By contrast, with only local dynamics, our model exhibits ordering at scales between the lattice spacing ℓ and the system size L , admitting a coarse-grained, hydrodynamic description.

Here we study a stripe formation phenomenon in a lattice gas model under a steady applied drive. We find non-equilibrium steady states with similar characteristics as the equilibrium phases described by the Landau-Brazovskii free energy for modulated phases. In particular, there is a phase transition between an ordered modulated (striped) phase at high particle density $\bar{\rho}$ and a disordered “microemulsion” phase at low densities in which the static structure factor has a characteristic peak. We develop a coarse-grained field theory for this process and show how our model captures two important limiting cases: The phase-separating binary mixture and a driven diffusive lattice gas. Similarly, many model systems also exhibit striped patterns when driven far from equilibrium. Examples include the venerable Ising system [16] and the 3-state Blume-Emery-Griffiths model [17, 18], especially when cast in the lattice gas language [19–24]. Subjected to a direct or a random drive

[10, 25–30], as well as various boundary conditions, these systems display stripes oriented parallel or perpendicular to the drive [31–35].

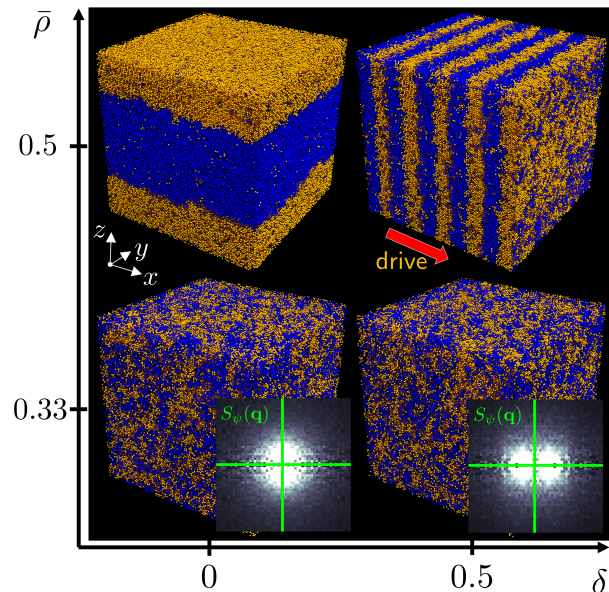


FIG. 2. Snapshots of steady states of the DWRLG for a $L \times L \times L$ system with $L = 100$ with equal mixtures of blue and orange particles. At high densities ($\bar{\rho} = 0.5$), the binary mixture phase separates either completely without a drive ($\delta = 0$) or into slabs with a drive ($\delta = 0.5$). The drive direction, $\hat{\mathbf{x}}$, is shown with a red arrow. At lower densities ($\bar{\rho} = 0.33$), the particles remain mixed. The static structure factors $S_\psi(\mathbf{q})$ for the disordered phases are shown as a function of $\mathbf{q} = (q_\parallel, q_\perp)$, where we average over the two directions perpendicular to the drive. Note the two maxima in the drive direction (inset on bottom right).

Granular [36] and colloidal systems [37] under an oscillatory drive can also form jammed clusters with the stripes running perpendicular to the drive direction. The dynamic instabilities observed in the sheared granular systems are reminiscent of the phenomenon described here [38, 39]. However, the stripes of granular particles typically coarsen over time, with the cluster sizes eventually approaching the system size. Conversely, our model shows stable structures at a characteristic scale λ^* at the longest time scales available in our simulations (10^8 Monte-Carlo steps, as discussed in the next section). Moreover, fully phase-separated states are observed to breakup until the clusters reach the characteristic size.

We consider the Widom-Rowlinson lattice gas with two species [40], A and B . The particles hop on a square or a simple cubic lattice, subjected to excluded-volume interactions. A and B particles cannot occupy nearest-neighbor sites, modelling a repulsive interaction between species.¹ The original, off-lattice version of this model with purely repulsive interactions may be

¹ Whether driven or not, this system on a one-dimensional pe-

mapped to a *single*-component gas with *attractive* interactions and exhibiting a vapor-liquid transition [47]. In the two-species case, the analog of the vapor-liquid transition is a phase separation of the two species when their density $\bar{\rho}$ (for equal proportions of the two species, $\bar{\rho}_A = \bar{\rho}_B = \bar{\rho}/2$) is larger than a critical value $\bar{\rho}^*$. At low densities $\bar{\rho}$, the particles remain mixed on average. These ordered and disordered equilibrium phases are shown in the left panels of Figs. 1 and 2 for two- and three-dimensional systems, respectively. A key quantity that characterizes the ordering process (into periodic structures) is the difference between the coarse-grained (local) particle densities $\psi(\mathbf{r}, t) = \rho_A(\mathbf{r}, t) - \rho_B(\mathbf{r}, t)$. We will study what happens to this density when the particles are “driven” uniformly, i.e., particle-hole exchanges in one direction are biased, as if the particles are placed in a uniform gravitational field. The effects of the drive are dramatic, as shown in the right panels of Figs. 1, 2. At low $\bar{\rho}$, we find a disordered phase with a characteristic peak in the static structure factor $S_\psi(\mathbf{q})$ (associated with the “charge field” ψ) along the drive direction (a “microemulsion”) and at high $\bar{\rho}$ we find an ordered phase of stripes (or slabs in 3D), reminiscent of a smectic liquid crystal.

To understand the structure of these phases, we begin with a free energy for the equilibrium case with no drive. It has been shown that without the drive, the lattice gas phase separation is in the Ising universality class [40] (with the underlying system being a diluted Ising one). As the number of particles remains fixed, we expect the charge field ψ to behave as a conserved “magnetization,” with the following coarse-grained free energy \mathcal{F} :

$$\mathcal{F} = \int d\mathbf{r} d\mathbf{r}' \psi(\mathbf{r}') G^{-1}(\mathbf{r} - \mathbf{r}') \psi(\mathbf{r}) + \int d\mathbf{r} V_I[\psi(\mathbf{r})], \quad (1)$$

where $G(\mathbf{r} - \mathbf{r}')$ is the Green’s function and $V_I[\psi(\mathbf{r})]$ are the higher-order interaction terms. For Ising systems, we expect that the relevant interaction is $V_I[\psi(\mathbf{r})] = u\psi^4$ and the (Fourier-transformed, inverse) Green’s function is the usual $G^{-1}(\mathbf{q}) = \tau + Cq^2$, with constants $C > 0$ and τ . Ignoring fluctuations, $\tau \propto \bar{\rho}^* - \bar{\rho}$ is our control parameter with $\tau > 0$ for the disordered phase (bottom left of Figs. 1, 2) and $\tau < 0$ for the phase separated phase (top left of Figs. 1, 2). The particle conservation

law would show up in the equation of motion for ψ , which must be of the conserved (model B [48]) form given by

$$\partial_t \psi(\mathbf{r}, t) = D \nabla^2 \frac{\delta \mathcal{F}}{\delta \psi} + \xi(\mathbf{r}, t), \quad (2)$$

with $\xi(\mathbf{r}, t)$ a Gaussian, conserved noise with correlations satisfying the fluctuation-dissipation theorem: $\langle \xi(\mathbf{r}, t) \xi(\mathbf{r}', t') \rangle = -2k_B T D \nabla^2 \delta(\mathbf{r} - \mathbf{r}') \delta(t - t')$, with D a diffusion constant, k_B the Boltzmann constant, and T the temperature. The mobility D and temperature T depend on the specific microscopic lattice rules, as well as the coarse-graining procedure. The important point to make here is that, without a drive, there is nothing to set the preferred scale q^* . The disordered phase ($\tau > 0$) has a structure factor (i.e., the Fourier-transform of the equal-time two point correlation) $S_\psi(\mathbf{q}) \propto (\tau + Cq^2)^{-1}$ peaked at the origin $q = |\mathbf{q}| = 0$. We verify this in our simulations in the bottom left panels of Figs. 1, 2 for two and three dimensions, respectively. In the ordered phase ($\tau < 0$), the binary mixture eventually fully phase separates. We can also see this in our simulations in the top left panels of Figs. 1, 2.

In the presence of a drive, novel features emerge. In particular, our model exhibits behavior reminiscent of systems with modulated phases in *equilibrium*, with some important differences. A modulated phase at equilibrium would have $S_\psi(\mathbf{q})$ with a maximum at a nonzero wavenumber: $S_\psi(\mathbf{q}) \propto [\tau + \kappa(|\mathbf{q}| - q^*)^2]^{-1}$, with $q^* = 2\pi/\lambda^*$ and λ^* the characteristic wavelength of the spatial modulation. In a scattering experiment, we would expect a large contribution at this wavenumber for any direction $\hat{\mathbf{q}}$. Conversely, in our model, the applied drive breaks the rotational symmetry of our system and the static structure factor $S_\psi(\mathbf{q})$ only has peaks along the drive direction, with $S_\psi(\mathbf{q}) \propto [\tau + \kappa_\parallel |\mathbf{q}_\parallel|^2 + \kappa_\perp (|\mathbf{q}_\perp| - q_\perp^*)^2]^{-1}$, where $q_\parallel = \mathbf{q} \cdot \hat{\mathbf{x}}_\parallel$ is the component of the wavevector parallel to and \mathbf{q}_\perp the component perpendicular to the drive direction $\hat{\mathbf{x}}_\parallel$. Here we use simulations and a coarse-grained field-theoretic approach to see how such a peculiar “microemulsion” phase may develop.

Another important limit worth mentioning is the out-of-equilibrium, low particle density $\bar{\rho}$ limit at non-zero drive. Here, we expect the inter-species repulsive interactions to be negligible and the lattice gas should reduce to the low density phase of a non-interacting driven diffusive system (DDS) [49–51]. The excluded volume condition, however, should still be relevant and appears as an interaction “along the drive” (see the term proportional to g below). The local particle density $\rho \equiv \rho(\mathbf{r}, t) = \rho_A(\mathbf{r}, t) + \rho_B(\mathbf{r}, t)$ would obey, in the frame moving with the mean particle velocity induced by the drive δ , the Langevin equation

$$\partial_t \rho = D [c \partial_\parallel^2 + \nabla_\perp^2] \rho + g \partial_\parallel [\rho^2] + \xi_\rho(\mathbf{r}, t), \quad (3)$$

where $\xi_\rho(\mathbf{r}, t)$ is a conserved noise satisfying $\langle \xi_\rho(\mathbf{r}, t) \xi_\rho(\mathbf{r}', t') \rangle = -2D(\tilde{c} \partial_\parallel^2 + \nabla_\perp^2) \delta(\mathbf{r} - \mathbf{r}') \delta(t - t')$, and c, \tilde{c} are coefficients reflecting the anisotropy in the

riodic lattice can be mapped (1-1) onto a ring with just one particle species hopping from one site to a nearest neighboring vacant site, with or without bias. Known as simple exclusion processes (SEPs) or asymmetric SEPs (ASEPs), the single species systems have been extensively studied [41–45]. (For a recent review, see, e.g., Ref. [46].) In particular, the stationary distribution is always uniform and the static properties are trivially drive-independent. As for the mapping, note that every allowed configuration of the Widom-Rowlinson lattice gas can be transformed into one in SEP/ASEP – by deleting a single vacancy from any cluster of holes lying between an A and a B particle, and then relabeling all the B particles as A ’s (say). It is straightforward to verify that, under this map, the rules for how one configuration changes to another is exactly preserved. Simulations data are entirely consistent with this picture.

diffusion and noise, respectively. Detailed balance is violated and a renormalization group analysis leads to anomalous diffusion (only in the direction of the drive) for $d \leq 2$ [49, 50]. We shall see that Eq. (3) represents the coarse-grained dynamics of our model in the important limiting case of low particle density and no repulsive interaction between particle species. As in DDS, Eq. (3) embodies a discontinuity singularity in the static structure factor $S(\mathbf{q})$, induced by detailed balance violation and the drive (see, e.g., Ref. [51]). Note, however, that it has no characteristic peak of the kind shown in Figs. 1, 2 (see insets in bottom right panels) [52, 53]. Moreover, it is known that single-species systems with attractive interactions do not form modulated phases, either. If any spatial structures emerge (e.g., stripes of high and low densities), they are invariably aligned *parallel* to the drive [25, 26, 51]. Thus, the behavior analyzed in the two-species model presented here is remarkable and unintuitive, especially in light of the limiting, well-studied cases described above.

The remainder of this paper is organized as follows: In the next section we define the model. Then, in Sec. III, we present simulation results on the disordered phase, including static structure factor calculations and the characteristic wavevector q_{\parallel}^* along the drive direction as a function of the drive δ . In Sec. IV, we derive a field theory corresponding to the lattice gas rules and show that, at the mean-field (Gaussian) level, it predicts some features of the disordered phase, yet missing the most prominent properties. Fluctuation corrections are discussed in Sec. V, and we show that a simple perturbative approach is able to capture, if only qualitatively, the essential behavior exhibited by our driven lattice gas. We conclude in Sec. VI and offer some directions for future investigation.

II. MODEL

We consider a lattice gas with two particle species, A (orange) and B (blue), that occupy sites $\mathbf{x} = \ell(i, j)$ on a square lattice or $\mathbf{x} = \ell(i, j, k)$ on a cubic lattice (with i, j, k integers), with ℓ the lattice spacing and L the length of the lattice. The space of allowed configurations is defined by the restrictions that (1) all particles occupy distinct sites, and (2) A - B nearest-neighbor pairs are prohibited, as shown in Fig. 3. We impose periodic boundary conditions in all directions. It is convenient to introduce spin variables $\sigma_{\mathbf{x}} = 0, \pm 1$ at each site, defined so:

$$\sigma_{\mathbf{x}} = \begin{cases} 1, & \mathbf{x} \text{ is occupied by } A \\ -1, & \mathbf{x} \text{ is occupied by } B \\ 0, & \mathbf{x} \text{ is empty.} \end{cases} \quad (4)$$

The numbers of A particles N_A , and of B particles N_B remain fixed, as do the average densities, $\bar{\rho}_{A,B} = N_{A,B}\ell^d/L^d$.

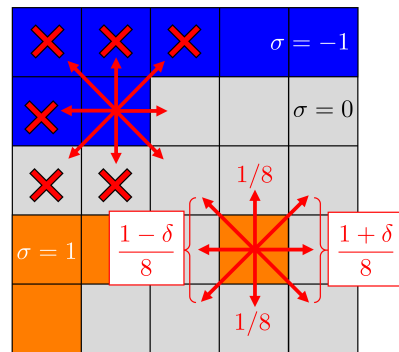


FIG. 3. Update rules for the DWRLG shown on a segment of a square lattice. Orange ($\sigma = 1$) and blue ($\sigma = -1$) particles can hop in one of eight directions with the indicated probabilities. A particle hops to the target site as long as it is unoccupied and is not a nearest neighbor of a particle of the opposite type. Some prohibited hops (red x's) are shown for a blue particle. The generalization to the cubic lattice is straightforward: there are then six nearest neighbors and twelve next-nearest neighbor sites to which particles can hop.

The hopping rules are those in Ref. [10] with $a = 1/4$: At each time step, we pick a random particle at location \mathbf{x} and move it to a nearest-neighbor (NN) or next-nearest-neighbor (NNN) site $\mathbf{x} + \Delta\mathbf{x}$ with the following probabilities:

$$\omega_{\mathbf{x} \rightarrow \mathbf{x} + \Delta\mathbf{x}} = \frac{1}{N_n} \begin{cases} 1 + \delta, & \Delta\mathbf{x} \cdot \hat{\mathbf{x}}_{\parallel} > 0 \\ 1 - \delta, & \Delta\mathbf{x} \cdot \hat{\mathbf{x}}_{\parallel} < 0 \\ 1, & \Delta\mathbf{x} \cdot \hat{\mathbf{x}}_{\parallel} = 0 \end{cases}, \quad (5)$$

where $0 \leq \delta \leq 1$ is the drive strength, $\hat{\mathbf{x}}_{\parallel}$ is the drive direction, and N_n is the number of NN and NNN sites. ($N_n = 8$ and 18 the square and simple cubic lattices, respectively.) The particle displacement is accepted subject to the restrictions mentioned above. Note that the rules are completely symmetric for the two species, so there is an “Ising-like” symmetry $\sigma_{\mathbf{x}} \rightarrow -\sigma_{\mathbf{x}}$ (so long as we keep the number of particles of each type the same, with $N_A = N_B$). After each such update, time advances by $1/N$, where $N = N_A + N_B$ is the total number of particles. We define one Monte-Carlo step (MCS) as having completed N such attempts and will label MCS by $n = 1, 2, \dots, N_{\text{MCS}}$. In our simulations, the runs involve typically N_{MCS} up to 5×10^7 , with the longest runs going up to 10^8 MCS. Measurements are taken typically after discarding the initial 4×10^6 MCS so that the system has arrived at a (reasonable) stationary state.

In equilibrium (no drive, $\delta = 0$), the model exhibits a phase transition at a critical density $\bar{\rho}^* = 0.617(1)$ and $\bar{\rho}^* = 0.3543(1)$ in two and three dimensions, respectively [40]. The transition is in the Ising universality class and describes the usual demixing transition of a binary mixture at sufficiently high densities. Examples of the disordered and ordered phases are shown in the left columns of Figs. 1 and 2. One may track the transition via the structure factor associated with the “charge”

order parameter field $\psi(\mathbf{r})$:

$$S_\psi(\mathbf{q}) = \frac{1}{L^d} \sum_{\mathbf{x}, \mathbf{r}} \langle \sigma_{\mathbf{x}} \sigma_{\mathbf{x}+\mathbf{r}} \rangle e^{i\mathbf{q}\cdot\mathbf{r}} = \frac{\langle |\sigma(\mathbf{q})|^2 \rangle}{L^d}, \quad (6)$$

where $\sigma(\mathbf{q})$ is the Fourier-transformed particle configuration $\sigma_{\mathbf{x}}$ and L^d the volume of the square ($d = 2$) or cubic ($d = 3$) lattice. For a phase with a characteristic length, we expect to find peaks in $S_\psi(\mathbf{q})$. We will analyze the formation of this ‘‘microemulsion peak’’ using simulation and a field-theoretic approach.

III. MICROEMULSIONS IN SIMULATIONS

We begin with simulation results that give the basic phenomenology of this system. We have simulated both two- and three-dimensional systems, but since it is easier to go to larger system sizes in two dimensions, this will be our primary focus. We will also primarily focus on the behavior of the system below the transition point ($\bar{\rho} < \bar{\rho}^*$) where we find a disordered ‘‘microemulsion’’ phase. As discussed in the previous section, although we do not have the distinct stripe order at low densities, the small fluctuating domains of particles in the system are characterized by a distinct length scale along the drive direction. This manifests as a peak in the structure factor $S_\psi(\mathbf{q})$ at $\mathbf{q} = (q_{\parallel}^*, 0)$. As one approaches the critical density $\bar{\rho} \rightarrow \bar{\rho}^*$, this peak value begins to diverge with the system size, as we develop the uniform stripe order seen in the top right panels of Figs. 1,2. For $\bar{\rho} < \bar{\rho}^*$, the position of the peak q_{\parallel}^* in the drive direction grows lin-

early with the drive δ in both two and three dimensions, as shown in Fig. 4. This is also reflected in the coarser texture of the microphase pattern for smaller δ , evident in the configuration snapshots.

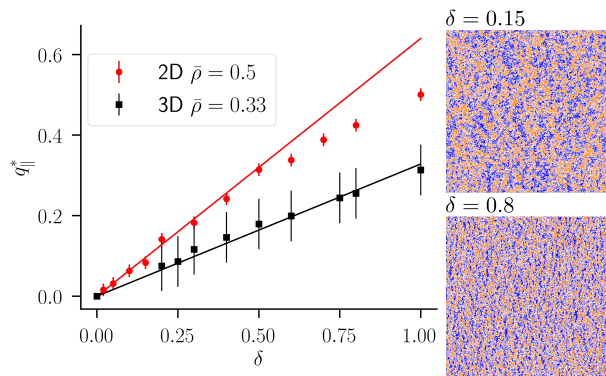


FIG. 4. Structure factor peak position q_{\parallel}^* for two- and three-dimensional systems in the microemulsion phase. Note that the peak varies linearly with the drive δ for small drives: $q_{\parallel}^* \propto \delta$. The error bars indicate $2\pi/L$ which sets the \mathbf{k} -space resolution ($L = 400$ for 2D and $L = 100$ for 3D). This linear variation of q_{\parallel}^* with δ in the disordered phase is consistent with our field-theoretic analysis. Typical system snapshots are shown for the square lattice on the right panels for $\bar{\rho} = 0.5$ and the indicated drive values δ .

In the previous work on this model [10], the conjectured simplest form of the static structure factor $S_\psi \equiv S_\psi(\mathbf{q})$, consistent with a dominant contribution at a nonzero $\mathbf{q} = (q_{\parallel}^*, 0)$, reads

$$S_\psi[\mathbf{q} = (q_{\parallel}, \mathbf{q}_{\perp})] = \frac{\nu_{\parallel} q_{\parallel}^2 + \nu_{\perp} |\mathbf{q}_{\perp}|^2 + \dots}{\tau_{\parallel} q_{\parallel}^2 + \tau_{\perp} |\mathbf{q}_{\perp}|^2 + q_{\parallel}^2 (|q_{\parallel} - q_{\parallel}^*|^2 + \gamma_{\times} q_{\parallel}^2 |\mathbf{q}_{\perp}|^2 + \gamma_{\perp} |\mathbf{q}_{\perp}|^4 + \dots)}, \quad (7)$$

with ellipses indicating corrections in higher powers of the momentum \mathbf{q} . The new interesting feature here is the cubic term, $-2q_{\parallel}^* |q_{\parallel}|^3$, in the denominator, which is responsible for the peak in the structure factor. The cubic term is unexpected from a mean field analysis and a naive continuum limit of the model, which yields only even powers of q_{\parallel} and no drive-dependence in any of the terms.² The cubic term also yields a linear kink in the static structure factor near the origin along the drive direction, as evidenced in Figs. 5 and 6, where we fit the conjectured form in Eq. (7) to simulation data for $\mathbf{q}_{\perp} = 0$. Note how well the form reproduces the features

at small q_{\parallel} . In two dimensions, we have verified that the kinked form is not a finite-size effect by checking that the form does not change as we vary the lattice size: $L = 100, 200, 400$. Also, as far as can be estimated from simulations, the peak exists for any $\delta > 0$. Our objective, then, is to explore how such a structure factor form may come about from a field-theoretic analysis of this model.

The static structure factors in two and three dimensions as a function of \mathbf{q} , both parallel and perpendicular to the drive, are shown in Fig. 5, as measured from simulations. It is worth noting that the static structure factors exhibit a characteristic jump discontinuity near the origin, captured by our conjectured form in Eq. (7) by setting $\nu_{\parallel}/\tau_{\parallel} \neq \nu_{\perp}/\tau_{\perp}$. We also see that the structure factors monotonically decrease along the direction q_{\perp} perpendicular to the drive for $q_{\parallel} = 0$. Along this direction, the structure factor is well-approximated by a simple Ornstein-Zernike form, corresponding to the $q_{\parallel} = 0$ case in Eq. (7).

² Also, the two-point correlation function must obey an underlying parity symmetry, which constrains it to be symmetric under $q_{\parallel} \rightarrow -q_{\parallel}$. The drive breaks this symmetry, but this feature can only appear at the level of three-point (or larger) correlation functions.

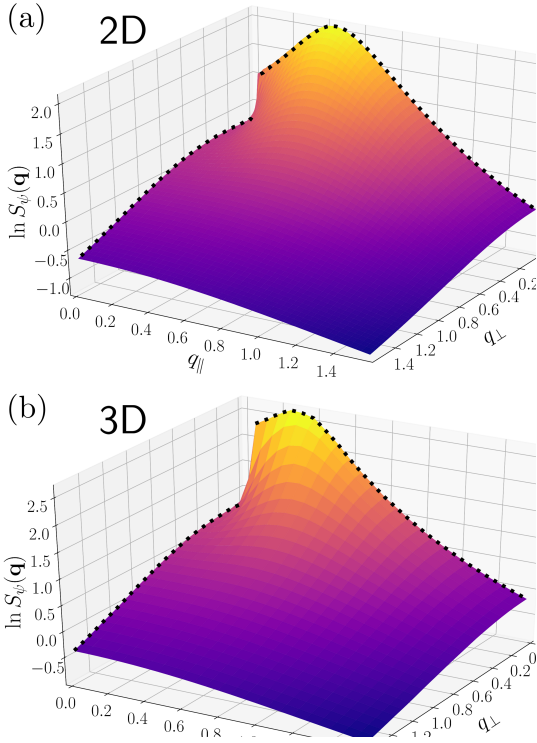


FIG. 5. Static structure factor $S_\psi(\mathbf{q})$ calculated from simulations for a drive $\delta = 0.8$ in the low-density phase in (a) two dimensions with $\bar{\rho} = 0.5$ (L^2 sites with $L = 400$) and (b) three dimensions, with $\bar{\rho} = 0.33$ (L^3 sites with $L = 100$). Note the jump discontinuity at the origin, characteristic of a driven diffusive system. The black dashed lines show the limiting forms of $S_\psi(\mathbf{q})$ for $\mathbf{q} = (q_{\parallel}, q_{\perp} = 0)$ and $\mathbf{q} = (q_{\parallel} = 0, q_{\perp})$. The $\mathbf{q} = (q_{\parallel} = 0, q_{\perp})$ direction has a smooth, featureless, monotonically-decreasing shape for the structure factor, while the other direction $\mathbf{q} = (q_{\parallel}, q_{\perp} = 0)$ has a peak at a non-zero characteristic wavenumber q_{\parallel}^* .

Before moving on, let us consider the static structure factor $S_\rho(\mathbf{q})$ for the density field $\rho \equiv \rho_A + \rho_B$ in two dimensions. This also has an interesting structure when the drive δ is applied, as can be seen in Fig. 7. Note how there is a kinked structure near $q_{\parallel} = 0$ that is of the *opposite sign* as $S_\psi(\mathbf{q})$ in Fig. 6. As shown in Fig. 7, the kinked increase at $q_{\parallel} = 0$ grows with increasing drive δ but starts to decrease for the largest drives. We will show that the kink near the origin likely comes from the fluctuation corrections in the field-theoretic description, just as for the charge fields. We should remark that $S_\rho(\mathbf{q})$ does not appear to exhibit any discernible signatures of the characteristic wavenumber q_{\parallel}^* . On closer examination, however, we can detect a shoulder in the $\delta = 0.5$ data, at roughly $2q_{\parallel}^*$. We suspect that, especially for the small δ systems, the enhancement manifest in S_ρ is mostly shrouded by the much larger effect near $q_{\parallel} = 0$ here. These properties are only true at small $\bar{\rho}$. In the high density, ordered phase (with $\bar{\rho} > \bar{\rho}^*$), $S_\rho(\mathbf{q})$ displays a peak at $\mathbf{q} = (q_{\parallel} = 2q_{\parallel}^*, q_{\perp} = 0)$, because high density stripes of A and B particles alternate, separated

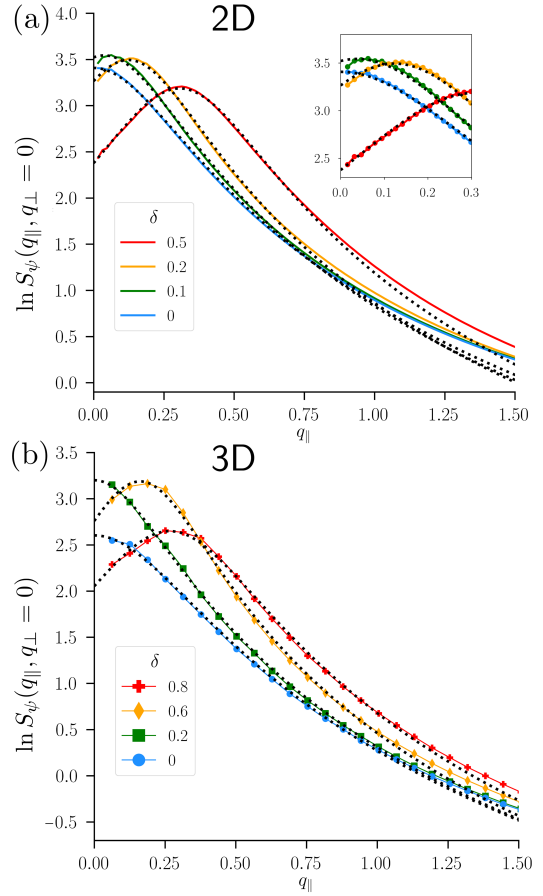


FIG. 6. Static structure factor at different values of the drive δ for the charge field $\psi = \rho_A - \rho_B$ as a function of q_{\parallel} for $|q_{\perp}| = 0$ in two- (a) and three- (b) dimensional systems with $L = 400$ and $L = 100$, respectively. In both cases, we are below the phase separation transition and have total particle densities $\bar{\rho} = 0.5$ in (a) and $\bar{\rho} = 0.33$ in (b). The dotted lines are fits to the form given by Eq. (7) (with three fitting parameters ν_{\parallel} , τ_{\parallel} , and q_{\parallel}^*). Because this form is only appropriate for small q where the details of the lattice structure are not important, we fit for data points between $0 < q_{\parallel} \lesssim 0.8$. Note that the structure factor develops a peak at a non-zero q_{\parallel} when $\delta > 0$. The inset in (a) has the same axes as the main plot and shows the structure factor shape near the origin where one finds a linear *kink*.

by low density regions (of many vacancies) [10].

Of course, the static structure factors $S_{\psi,\rho}(\mathbf{q})$ display only part of the interesting behavior we observe. The dynamic structure factors $S_{\psi,\rho}(\mathbf{r}, n)$ for the charge and density fields are also important, as they directly capture not only the diffusive properties of the particles, but also the advection. In particular, we may measure the unequal time correlations given by

$$S_\psi(\mathbf{r}, n) = \frac{1}{L^d} \sum_{\mathbf{x}, t} \langle \sigma_{\mathbf{x}}(t) \sigma_{\mathbf{x}+\mathbf{r}}(t+n) \rangle \quad (8)$$

$$S_\rho(\mathbf{r}, n) = \frac{1}{L^d} \sum_{\mathbf{x}, t} [\langle |\sigma_{\mathbf{x}}(t)| |\sigma_{\mathbf{x}+\mathbf{r}}(t+n)| \rangle - \bar{\rho}^2], \quad (9)$$

with $\sigma_{\mathbf{x}}(t)$ the spin configuration at time step t and lat-

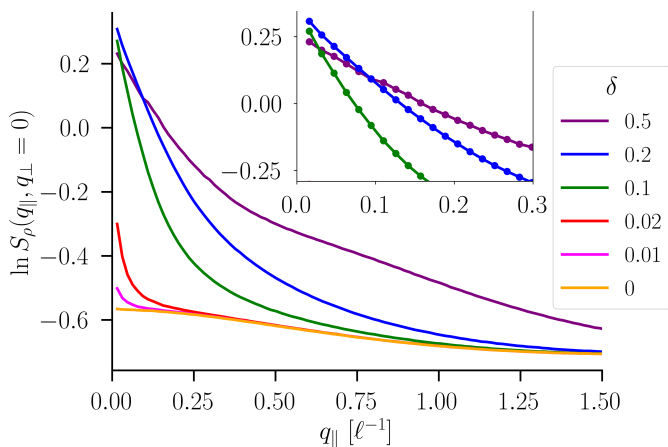


FIG. 7. Static structure factor $S_\rho(\mathbf{q})$ [with $\mathbf{q} = (q_\parallel, q_\perp)$] of the density field $\rho = \rho_A + \rho_B$, as a function of q_\parallel , with $q_\perp = 0$, measured in simulations for drives δ as indicated. S_ρ is calculated using a two-dimensional system with $L^2 = 400^2$ lattice sites at an average particle density of $\bar{\rho} = 0.5$ (equal fractions of A and B particles). The inset, which has the same axes as the main plot, shows a detail of the small- q_\parallel region. S_ρ has a cusped, sharp increase near $q_\parallel = 0$, consistent with a logarithmic divergence. Unlike in the case of the charge structure factors S_ψ shown in Fig. 6(a), we do not find a peak here.

tice site \mathbf{x} [see Eq. (4)], and $\bar{\rho}$ the average particle density in the system (total number of A and B particles divided by the total number of lattice sites). The angular brackets $\langle \dots \rangle$ denote an average over many simulation runs. The results for the low density phase in two dimensions are shown in Fig. 8.

Note that the charge and density dynamic structure factors have very different behaviors: The peaks of the charge field structure factor $S_\psi(\mathbf{r}, n)$ broaden more slowly and move more rapidly compared to the density field structure factor $S_\rho(\mathbf{r}, n)$. This is consistent with a larger characteristic velocity and a smaller diffusivity for the charge field. Moreover, the shape of these structure factors is approximately Gaussian. We shall justify this particular form and derive these properties in the following section when we explore the field-theoretic formulation of this model.

IV. COARSE-GRAINED FIELD-THEORETIC MODEL

To understand how these unusual properties arise from being driven, even if only qualitatively, we will attempt an approach based on coarse-graining our discrete lattice system to a continuum field-theory. Starting with a set of stochastic update rules, such as those described by Eq. (5), it is straightforward to derive a master equation for the evolution of the probability $P(\{\sigma_{\mathbf{x}}\}, t)$ of observing a particular lattice configuration $\{\sigma_{\mathbf{x}}\}$ at time t . From here, there are standard procedures for converting that description into one based on a Langevin equa-

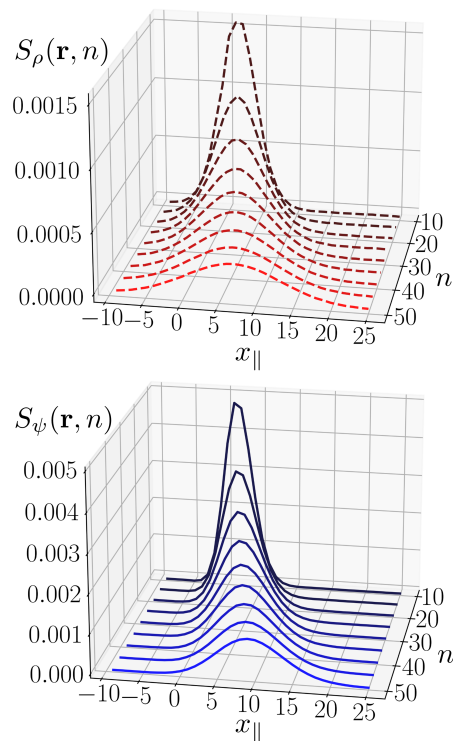


FIG. 8. Dynamic (real-space) structure factors [defined in Eqs. (8,9)] calculated from a two-dimensional simulation with equal fractions of A and B particles with $\bar{\rho} = 0.1$ and $\delta = 0.3$ (system size $L = 50$). The factors are evaluated along the drive direction $\mathbf{r} = (x_\parallel, 0)$. The charge field structure factor $S_\psi(\mathbf{r}, n)$ (lower panel) propagates more rapidly and spreads more slowly than the density field structure factor, $S_\rho(\mathbf{r}, n)$ (upper panel). Both have Gaussian shapes. These properties can be understood within a field-theoretic framework.

tion for coarse-grained density fields $\rho_{A,B}(\mathbf{x}, t)$. A common approach employs the Martin-Siggia-Rose-Janssen-de Dominicis (MSRJD) formalism [54–56] which translates these equations into a field-theoretic, “dynamical action” \mathcal{J} involving both the $\rho_{A,B}$ ’s and corresponding “response fields” $\hat{\rho}_{A,B}(\mathbf{x}, t)$. Following the general procedure for particle hopping models [57], the dynamical action reads

$$\mathcal{J}[\rho_{A,B}, \hat{\rho}_{A,B}] = \sum_{\alpha=A,B} \int dt \left\{ \sum_{\mathbf{x}} \hat{\rho}_\alpha \partial_t \rho_\alpha + \sum_{\langle \mathbf{x}\mathbf{y} \rangle} W_{\mathbf{x} \rightarrow \mathbf{y}}^\alpha \left[1 - e^{\hat{\rho}_\alpha(\mathbf{x}) - \hat{\rho}_\alpha(\mathbf{y})} \right] \right\}, \quad (10)$$

where $W_{\mathbf{x} \rightarrow \mathbf{y}}^\alpha$ are the hopping rates from site \mathbf{x} to \mathbf{y} for particles of type $\alpha = A, B$ [which can be gleaned from the ω ’s in Eq. (5)]. These W ’s encode both the hopping and the exclusion rules and must vanish for any prohibited hops (see Fig. 3). We sum over all pairs of NN and NNN sites $\langle \mathbf{x}\mathbf{y} \rangle$. From here, the average over many stochastic realizations of the particle system may be computed for any functional of the densities $\mathcal{O}(\{\rho_{A,B}\})$

(“observables”) using the action \mathcal{J} via:

$$\langle \mathcal{O}(\{\rho_{A,B}\}) \rangle = \frac{1}{\mathcal{Z}} \int \mathcal{D}\rho_{A,B} \mathcal{D}\hat{\rho}_{A,B} \mathcal{O}(\{\rho_{A,B}\}) e^{-\mathcal{J}}, \quad (11)$$

with \mathcal{Z} providing normalization. Also, note that the Euler-Lagrange equations associated with extremizing \mathcal{J} (with an appropriate interpretation of the response fields $\hat{\rho}_{A,B}$) lead us to Langevin equations for the densities $\rho_{A,B}(\mathbf{x}, t)$. As these are more easily grasped intuitively, we will present the field theoretic formulation in such terms [see Eqs. (12) below].

A second method (Doi-Peliti [58, 59]) of deriving a coarse-grained description of the dynamics and the dynamical action \mathcal{J} involves reformulating the master equation for $P(\{\sigma_{\mathbf{x}}\}, t)$ using a Fock space where the probability distribution P is encoded in a multi-particle state. Then, using a coherent state path integral representation of the master equation, one is able to derive a dynamical action of the same form as Eq. (10). In principle, these two methods yield equivalent field theories [57], but the mapping is non-trivial. Also, a special difficulty in our case is that both the excluded volume constraint and the A, B particle next-nearest neighbor exclusion rule are not easily incorporated. One possibility, introduced by van Wijland [60], is to apply the exclusion rules at the level of the master equation, which is exact but difficult to interpret when we coarse-grain. A review can be found in, e.g., Ref. [61]. This procedure is quite involved and some details are provided in Appendix A for the interested reader.

Encouragingly, after taking the continuum limit and expanding around small density fluctuations, both the Doi-Peliti and MSRJD methods yield the same structure for the field theory, with minor variations in the dependencies of the coupling constants on the microscopic parameters $\bar{\rho}_{A,B}$ and δ . In the following we use results from the Doi-Peliti approach using van Wijland’s method for excluded volume interactions.

In the paradigm of this coarse-grained continuum description, we assume the density fields ρ_{α} and their corresponding response fields $\hat{\rho}_{\alpha}$ are slowly varying in space and time (\mathbf{r}, t) . To construct a perturbation theory and compare to our simulation results, we transform to more convenient fields (i.e., ones which diagonalize the quadratic part in \mathcal{J} : the total density $\rho \equiv \rho_A + \rho_B$ and the “charge” order parameter $\psi \equiv \rho_A - \rho_B$). We have to expand the fields ρ and ψ around some uniform concentrations $\bar{\rho}$ and $\bar{\psi}$ which, along with the drive δ , are our control parameters in the simulations. With the replacements $\rho = \bar{\rho} + \phi_+$ and $\psi = \bar{\psi} + \phi_-$, we find that, to leading order in the fluctuations ϕ_{\pm} and the averages, the Langevin equations read

$$\begin{cases} \partial_t \phi_+ = D_+ \nabla^2 \phi_+ - v_+ \partial_{\parallel} \phi_+ - u_+ \bar{\psi} \partial_{\parallel} \phi_- \\ \quad + \frac{g_+}{2} \partial_{\parallel} (\phi_+^2) - \frac{g_-}{2} \partial_{\parallel} (\phi_-^2) + \xi_+ \\ \partial_t \phi_- = D_- \nabla^2 \phi_- - v_- \partial_{\parallel} \phi_- \\ \quad + u_- \bar{\psi} \partial_{\parallel} \phi_+ + g_0 \partial_{\parallel} (\phi_- \phi_+) + \xi_- \end{cases}, \quad (12)$$

where the coefficients of all the terms carry appro-

priate units of space (the lattice spacing ℓ) and time (MCS) which will be suppressed. With this understanding, we find (the leading constants and lowest-order corrections in powers of $\bar{\rho}$ and $\bar{\psi}$ for) the diffusion coefficients $D_{\pm} \approx 3/8$ and the velocities $v_{\pm} = \bar{v} \pm v_d/2$ with average $\bar{v} = (v_+ + v_-)/2 \approx \delta(3 - 22\bar{\rho})/4$ and the difference $v_d = v_+ - v_- \approx -5\bar{\rho}\delta/2$. The other velocities, $u_+ \approx 7\delta/4$ and $u_- \approx 3\delta/4$, do not appear in this study, as we focus on neutral systems ($\bar{\psi} = 0$) only. While $\nabla^2 = \nabla_{\perp}^2 + \partial_{\parallel}^2$ represents isotropic diffusion, there are DDS-like anisotropic, non-linear couplings $g_- = \sqrt{2}\delta$, $g_+ = 4\sqrt{2}\delta$, and $g_0 = 3\sqrt{2}\delta$ all proportional to the drive δ . As we shall see, these interaction terms will generate anisotropy in the diffusion terms. We also find conserved noises for both the charge and density, with correlations given by: $\langle \xi_+ \xi_+ \rangle = -2N_+ \bar{\rho} \nabla^2 \delta(\mathbf{r} - \mathbf{r}') \delta(t - t')$ and $\langle \xi_- \xi_- \rangle = -2N_- \bar{\rho} \nabla^2 \delta(\mathbf{r} - \mathbf{r}') \delta(t - t')$, with $N_{\pm} \approx 3/8$. When $\bar{\psi} \neq 0$, there are nonzero cross-correlations, $\langle \xi_+ \xi_- \rangle = -2N_{+-} \bar{\psi} \nabla^2 \delta(\mathbf{r} - \mathbf{r}') \delta(t - t')$, with $N_{+-} \approx 3/8$. While it is of course possible to obtain more detailed expressions for the coupling constants in terms of the microscopic control parameters $\bar{\rho}$, $\bar{\psi}$, and δ , they are not needed for our objective of understanding the coarse-grained features of the dynamics at small particle density $\bar{\rho}$.

Note that when either of the two species vanishes, so that $\rho = \psi = \rho_{A,B}$, both equations in Eq. (12) reduce to the DDS Langevin equation in Eq. (3) with $g = g_0 = g_+ - g_-$ as the derivative coupling. This is an important limiting case as we would expect our model to reduce to the single-species DDS when we remove the repulsive interactions between particle species. The other important case is $\delta = 0$, where we would expect phase separation of the A and B particles at sufficiently high densities. In this case, Eq. (12) reduces to a pair of independent diffusion equations. To understand the system at higher particle densities, higher-order terms in the fields ϕ_{\pm} need to be included. If we further assume the density fluctuations ϕ_+ relax faster than the charge ϕ_- and integrate out the former, the effective equation for the latter reduces to an Ising system with conserved dynamics (model B). However, this is a crude approximation and a more careful analysis would involve accounting for both fields ϕ_{\pm} and considering the action at high particle densities $\bar{\rho}$. Such a line of pursuit is beyond the scope of this paper. Here we focus on the low-density phase, and defer a detailed analysis of phase separation to future work.

We now discuss the dynamic action associated with the Langevin equations, Eqs. (12). To compare with simulation results, we impose equal average densities ($\bar{\psi} = 0$) and find that, up to cubic terms in the fields

and leading order in spatial derivatives, the action reads

$$\begin{aligned} \mathcal{J} = \int d\mathbf{r} dt \left\{ \sum_{a=\pm} \left[\hat{\phi}_a (\partial_t - D_a \nabla^2 + v_a \partial_{\parallel}) \phi_a \right. \right. \\ \left. \left. + \bar{\rho} N_a \hat{\phi}_a \nabla^2 \hat{\phi}_a \right] + g_0 \phi_- \phi_+ \partial_{\parallel} \hat{\phi}_- + \frac{g_+}{2} \phi_+^2 \partial_{\parallel} \hat{\phi}_+ \right. \\ \left. - \frac{g_-}{2} \phi_-^2 \partial_{\parallel} \hat{\phi}_+ \right\}. \end{aligned} \quad (13)$$

In the disordered phase, $\bar{\rho} < \bar{\rho}^*$, the diffusion constants D_{\pm} are both positive. A scaling analysis (taking $\mathbf{r} \rightarrow \Lambda \mathbf{r}$) shows that the scaling dimension of the drive couplings $g_{0,\pm}$ is $1 - d/2$, so that the upper critical dimension is $d_c = 2$ for the $\bar{\rho} < \bar{\rho}^*$ regime, as it is for the single-species DDS at low densities [50]. We therefore conclude that higher-derivative coupling terms are irrelevant in the renormalization group sense.

Next, we set up a diagrammatic expansion using the action of Eq. (13). There are two kinds of propagators generated by the quadratic terms in the fields ϕ_{\pm} and $\hat{\phi}_{\pm}$. In the Fourier domain, we have the (bare) correlation functions $\langle \phi_{\pm}(\mathbf{q}, \omega) \phi_{\pm}(\mathbf{q}', \omega') \rangle \equiv C_{\pm}(\mathbf{q}, \omega) \delta(\mathbf{q} + \mathbf{q}') \delta(\omega' + \omega)$ and the response functions $\langle \hat{\phi}_{\pm}(\mathbf{q}, \omega) \phi_{\pm}(\mathbf{q}', \omega') \rangle \equiv G_{\pm}(\mathbf{q}, \omega) \delta(\mathbf{q} + \mathbf{q}') \delta(\omega' + \omega)$. Using dotted and solid lines for the density and charge fluctuations, respectively, we denote these by the following:

$$\begin{cases} G_{\pm} = \frac{1}{-i[\omega - v_{\pm} q_{\parallel}] + D_{\pm} |\mathbf{q}|^2} & \text{.....} \blacktriangleright \text{.....} \\ C_{\pm} = \frac{2N_{\pm} \bar{\rho} |\mathbf{q}|^2}{[\omega - v_{\pm} q_{\parallel}]^2 + [D_{\pm} |\mathbf{q}|^2]^2} & \text{.....} \text{-----} \end{cases}, \quad (14)$$

Both the numerators for C_{\pm} and the denominators for G_{\pm} , C_{\pm} have corrections in higher powers of $|\mathbf{q}|^2$, starting with $|\mathbf{q}|^4$. In the disordered phase $\bar{\rho} < \bar{\rho}^*$, the quartic momentum terms are irrelevant. We will be interested in finding fluctuation corrections that generate a peak in the structure factor, along with a possible kink near the origin, which cannot exist in a mean-field theory. The reason is simple: Any odd terms in q_{\parallel} are always imaginary and give contributions to the velocity terms proportional to the drive δ . Therefore, they are always removed by an appropriate choice of co-moving frame for the fields ϕ_{\pm} . We can see this explicitly when we calculate the static structure factors $S_{\rho, \psi}(\mathbf{q})$ directly from the correlation functions C_{\pm} .

$$\begin{aligned} S_{\rho, \psi}(\mathbf{q}) &= \int_{-\infty}^{\infty} \frac{d\omega}{2\pi} \frac{2f_N^{(\pm)}(\mathbf{q})}{[\omega - f_v^{(\pm)}(\mathbf{q})]^2 + [f_D^{(\pm)}(\mathbf{q})]^2} \\ &= \frac{f_N^{(\pm)}(\mathbf{q})}{|f_D^{(\pm)}(\mathbf{q})|} \end{aligned} \quad (15)$$

In this expression, we have included the higher-order corrections for C_{\pm} appearing in the velocity $[f_v^{(\pm)}(\mathbf{q}) \equiv v_{\pm} q_{\parallel} + C_v^{(\pm)} |\mathbf{q}|^2 q_{\parallel} + \dots]$, the noise $[f_N^{(\pm)}(\mathbf{q}) \equiv N_{\pm} \bar{\rho} |\mathbf{q}|^2 + C_N^{(\pm)} \bar{\rho} |\mathbf{q}|^4 + \dots]$, and the diffusion $[f_D^{(\pm)}(\mathbf{q}) \equiv D_{\pm} |\mathbf{q}|^2 + C_D^{(\pm)} |\mathbf{q}|^4 + C_D^{\times} q_{\parallel}^2 q_{\perp}^2 + \dots]$. Here, $C_D^{(\pm)} \approx 3/16$ and

$C_D^{\times} \approx 3/8$, to leading order in $\bar{\rho}$. We see that $f_v^{(\pm)}(\mathbf{q})$ does not contribute to the static structure factors, so that odd powers of \mathbf{q} never appear. Terms like $|q_{\parallel}|^3$ in Eq. (7) must be sought from the fluctuation corrections induced by the interaction terms (cubic and higher-order in the fields) in the action \mathcal{J} [Eq. (13)].

Before analyzing fluctuation corrections, it is worth comparing the results of this field-theoretic approach to simulation data for low densities and small drive, where we expect good agreement with the ‘‘bare’’ correlation functions in Eq. (14). Specifically, after inverting back to (\mathbf{r}, t) , they correspond to Gaussians for $S_{\psi, \rho}(\mathbf{r}, t)$. In particular, along the drive direction $[\mathbf{r} = (x_{\parallel}, 0)]$, we find

$$S_{\rho, \psi}[\mathbf{r}, t] = \frac{N_{\pm} \bar{\rho}}{4\pi D_{\pm}^2 t} \exp \left[-\frac{(x_{\parallel} - v_{\pm} t)^2}{4D_{\pm} t} \right], \quad (16)$$

with the plus (minus) signs for the density (charge) case. This form is consistent with the simulation results shown in Fig. 8. Fitting these curves to drifting Gaussians, we can extract simulation values for v_{\pm}/δ and D_{\pm} . These can be compared with theoretical values, estimated beyond the lowest order in $\bar{\rho}$ by using the Doi-Peliti approach (see Appendix A): $v_{\pm}/\delta = e^{-3\bar{\rho}}[(1 - \bar{\rho})(1 + 2e^{\bar{\rho}/2}) \mp 2\bar{\rho}(2 + 3e^{\bar{\rho}/2})]/4$ and $D_{\pm} = e^{-3\bar{\rho}}(1 + 2e^{\bar{\rho}/2} \pm \bar{\rho}(3 + 5e^{\bar{\rho}/2}))/8$. The comparison is shown in Fig. 9 with v_{+}/δ , D_{+} indicated by dashed red lines and v_{-}/δ , D_{-} , by solid blue. Given that we relied on only the lowest possible order in the field-theoretic approach, it is remarkable how well the predictions fare, especially at small $\bar{\rho}$. Note that at larger densities $\bar{\rho}$ that approach the phase transition, our mean-field results predict a vanishing D_{-} , which is not observed in the simulation results [see Fig. 9(b)]. We thus expect the perturbation theory for the fluctuation corrections developed in the next section to break down near the phase transition, where other techniques (e.g., the renormalization group) have to be employed.

We end this section with some comments on the aspects of our driven lattice gas which may be understood in terms of a ‘‘bare’’ theory. The velocities of the two fields are different, with that of the density-field being lower: $v_{+} < v_{-}$. Though the theoretical value seems to vanish at some special $\bar{\rho}$, it is unclear if this point is of any physical significance. We should remind ourselves that this is the velocity of the *fluctuations* and not the density itself. Such is a common experience in traffic, where local jams (fluctuations of higher density) are often observed to travel ‘‘backwards’’ from the direction of the drive. The two diffusion coefficients D_{\pm} also differ in general. Though $D_{+} > 0$ for all values of $\bar{\rho}$, D_{-} vanishes at some point, as mentioned above. Ordinarily (in both equilibrium systems and DDS), this is a signal of criticality and onset of phase separation. However, a vanishing coefficient of q^2 cannot describe the transition into stripes observed. Instead, there must be a divergence of $S_{\rho}(\mathbf{q})$ at $|q_{\parallel}| = 2q_{\parallel}^*$ (to accompany the divergence of S_{ψ} at $|q_{\parallel}| = q_{\parallel}^*$). Nevertheless, for densities far below criticality, this theory does capture the drifting and diffusive behavior of both kinds of fluctuations.

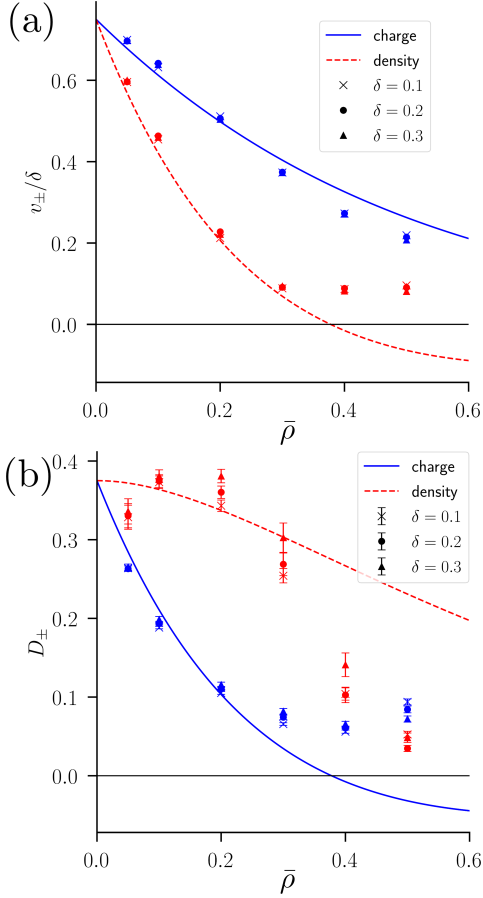


FIG. 9. Velocities v_{\pm} (a) and diffusivities D_{\pm} (b) associated with the dynamic structure factors for the charge (–) and density (+) fields, obtained by fitting the forms in Eq. (14) to simulation data for two-dimensional systems ($L = 50$, equal fractions of A and B particles) total particle density $\bar{\rho}$. The lines (red dashed and solid blue) show the theoretical results using the Doi-Peliti approach. We calculate these quantities for different values of the drive δ and show that the simulation results are consistent with the mean-field theory prediction that v_{\pm} are proportional to δ while D_{\pm} are independent of the drive δ .

Note that the difference in velocities $v_d = v_+ - v_-$ being non-zero is a key feature of the model. As a result, it is not possible to choose a co-moving frame in which *both* densities suffer no drift. In technical terms, we cannot eliminate both drift terms from the Langevin equations for ϕ_{\pm} , Eq. (12), so that one of them must be involved when we consider the fluctuation corrections. The presence of a drift term is not only a major difference between the field-theoretic formulation for our model and that for DDS [52, 53], but also appears to be the key ingredient for the emergence of spatial structures periodic along the drive.

To summarize, mean-field theory (i.e., the quadratic part of \mathcal{J}) provides us with static structure factors of

the form

$$S_{\rho,\psi}(\mathbf{q}) = \frac{N_{\pm}\bar{\rho}|\mathbf{q}|^2}{D_{\pm}|\mathbf{q}|^2 + C_D^{(\pm)}|\mathbf{q}|^4 + C_D^{\times}q_{\parallel}^2q_{\perp}^2}, \quad (17)$$

which is clearly inadequate for generating the characteristic “microemulsion” peaks in S_{ψ} when $\delta > 0$. These peaks can only arise from the fluctuation corrections (with $v_d \neq 0$ playing a key role), which will be our focus in the next section.

V. FLUCTUATION CORRECTIONS

Corrections due to fluctuations can be developed using a perturbative approach, starting with the quadratic terms in the action \mathcal{J} [i.e., a “free” field theory, with the correlation functions in Eq. (14)]. In this work, we restrict our attention to how these two-point functions are modified by the cubic terms in \mathcal{J} , i.e., those with $g_{0,\pm} \propto \delta$: $\langle \dots \rangle$ for g_- , $\langle \dots \rangle$ for g_0 , and $\langle \dots \rangle$ for g_+ , with the arrows indicating the response fields on which we place the derivative ∂_{\parallel} . Further, we will focus on finding corrections to just the *static* structure factors for $d = 2$. Thus, we will concentrate only on the self-energies $\Sigma_{\pm} \equiv \Sigma_{\pm}(\mathbf{q}, \omega)$ (which will correct the propagators for the density and charge fields, respectively) and the corresponding corrections to the noise correlations, $\eta_{\pm} \equiv \eta_{\pm}(\mathbf{q}, \omega)$. These enter into the fluctuation-corrected causal propagators $\bar{G}_{\pm} \equiv \bar{G}_{\pm}(\mathbf{q}, \omega)$ via Dyson’s equation:

$$\begin{aligned} \bar{G}_{\pm}^{-1} &= G_{\pm}^{-1} - \Sigma_{\pm} \\ &= -i(\omega - v_{\pm}q_{\parallel} + \text{Im} \Sigma_{\pm}) + D_{\pm}|\mathbf{q}|^2 - \text{Re} \Sigma_{\pm} \end{aligned} \quad (18)$$

and the corrected noise correlations via

$$\bar{N}_{\pm}(\mathbf{q}, \omega) = N_{\pm}|\mathbf{q}|^2 + \eta_{\pm}(\mathbf{q}, \omega). \quad (19)$$

These corrections contribute to the static structure factors through the expression:

$$S_{\rho,\psi}(\mathbf{q}) = \int \frac{d\omega}{\pi} \left[\frac{N_{\pm}|\mathbf{q}|^2 + \eta_{\pm}}{(\omega - v_{\pm}q_{\parallel} + \text{Im} \Sigma_{\pm})^2 + (D_{\pm}|\mathbf{q}|^2 - \text{Re} \Sigma_{\pm})^2} \right]. \quad (20)$$

Note that if we ignore the ω dependence in Σ and η , then the integration over ω eliminates $v_{\pm}q_{\parallel} - \text{Im} \Sigma_{\pm}$ and has the same effect as evaluating the corrections in the co-moving frame $\omega = v_{\pm}q_{\parallel}$ while keeping only $\text{Re} \Sigma_{\pm}$. In the analysis presented below, we will avoid such an uncontrollable approximation and compute the integral numerically instead. The details of this calculation are quite involved and are deferred to Appendix B for the interested reader. In this section, we will provide a brief overview of the various ingredients and steps, ending with the results and a discussion of their implications.

In two dimensions, we can generally expect (logarithmic) divergence at both the UV and IR ends. As we plan to compare our results to simulation data on a finite lattice, we will simply impose an UV cutoff, Λ , and evaluate at non-zero wavenumbers [specifically, $q_{\parallel} \sim O(1/L)$]. In fact, since both densities are conserved, $S_{\rho,\psi}(\mathbf{q} = 0)$ are fixed [10].

Turning first to the self-energy $\Sigma_- \equiv \Sigma_-(\mathbf{q}, \omega)$ for the charge field, we see that the lowest order corrections (i.e., with one loop, $\propto \delta^2$) are, in terms of diagrams, given by

$$\Sigma_-(\mathbf{q}, \omega) = \text{---} \circ \text{---} + \text{---} \circ \text{---} \quad (21)$$

$$= \int d\omega_k d\mathbf{k} \{g_0 g_- \dots + g_0^2 \dots\}. \quad (22)$$

The key feature of the loop integration is the mixing of the propagators for the charge and density fields [dashed and solid lines in Eq. (21)] which prevents us from eliminating the linear drift terms $v_{\pm} k_{\parallel}$ in both propagators simultaneously. In the usual single-species DDS case, for example, a Galilean transformation into a co-moving frame removes the linear drift term. This is not possible here as the charge and density fields have *different* characteristic velocities v_{\pm} . Indeed, as will be shown below, $v_d \equiv v_+ - v_-$ plays the key role for characterizing the periodic structures. A similar phenomenon occurs in a model for drifting crystals treated in Ref. [62], which also has two scalar fields with different drift velocities.

Substituting in the propagators from Eq. (14) and evaluating the integrals, we find, to leading order in the average density $\bar{\rho}$,

$$\begin{aligned} \Sigma_- \approx g_0 \frac{\bar{\rho} \bar{N} v_d q_{\parallel}}{16\pi \bar{D}^3} & \left\{ \left[\frac{2(g_- - g_0) q_{\parallel}}{q_c} - \frac{i(g_- + g_0)}{2} \right] \right. \\ & \times \ln \left[\frac{(4\Lambda)^2}{2i(\bar{v} q_{\parallel} - \omega)/\bar{D} + q_c^2 + |\mathbf{q}|^2} \right] + i(g_- + g_0) \left. \right\}, \end{aligned} \quad (23)$$

where

$$q_c \equiv \frac{v_d}{2\bar{D}} \quad (24)$$

is a crossover wavenumber that will be prominent in our discussions below. From this complex expression, it is instructive to study the real and imaginary parts of Σ_- (with real \mathbf{q} and ω) separately, as they enter into the diffusive and drift parts of Eq. (20), respectively. As discussed above, $\text{Re} \Sigma_-$ plays a more significant role for

S_{ψ} and it reads

$$\begin{aligned} \text{Re} \Sigma_- = \frac{\bar{N} \bar{\rho} g_0}{32\pi \bar{D}^2} & \left\{ \right. \\ & (g_- - g_0) q_{\parallel}^2 \ln \left[\frac{(4\Lambda)^4}{[2(\bar{v} q_{\parallel} - \omega)/\bar{D}]^2 + (q_c^2 + |\mathbf{q}|^2)^2} \right] \\ & \left. - 2(g_- + g_0) q_c q_{\parallel} \tan^{-1} \left[\frac{2(\bar{v} q_{\parallel} - \omega)/\bar{D}}{q_c^2 + |\mathbf{q}|^2} \right] \right\}. \end{aligned} \quad (25)$$

The first term in the curly braces, proportional to q_{\parallel}^2 , would renormalize the diffusivity D_- in the drive direction. It introduces a DDS-like anisotropy and leads to a potential discontinuity in the static structure factor at $\mathbf{q} = 0$. The second term, with coefficient $q_c q_{\parallel} \propto v_d q_{\parallel}$, has no DDS analog. Of course, an integration over ω is needed to obtain the static $S_{\psi}(\mathbf{q})$. But, as noted above, we can find a rough estimate of its effect by evaluating this term in the co-moving frame (by setting $\omega = v_- q_{\parallel}$ in this case). The result is $\propto q_c q_{\parallel} \tan^{-1} [q_c q_{\parallel} / (q_c^2 + |\mathbf{q}|^2)]$, confirming that it is necessarily even in q_{\parallel} . Yet, it provides the signal of a crossover: For small q_{\parallel} , it starts as q_{\parallel}^2 , but it behaves as $|q_{\parallel}|$ for values around q_c (where the \tan^{-1} is slowly varying). This is the property that offers the possibility of a maximum in S_{ψ} , as we shall see. By contrast, the imaginary part, $\text{Im} \Sigma_-$, does not affect S_{ψ} qualitatively and the result may be found Appendix B.

Turning to the correction to the noise in $\bar{N}_-(\mathbf{q}, \omega) = N_- \bar{\rho} |\mathbf{q}|^2 + \eta_-$, we see that the relevant diagram is

$$\eta_- = \text{---} \circ \text{---} = \int d\omega_k d\mathbf{k} \{g_0^2 \dots\} \quad (26)$$

with the result

$$\eta_- \approx g_0^2 \frac{\bar{N}^2 \bar{\rho}^2}{8\pi \bar{D}^3} q_{\parallel}^2 \ln \left[\frac{(4\Lambda)^4}{[2(\bar{v} q_{\parallel} - \omega)/\bar{D}]^2 + (q_c^2 + |\mathbf{q}|^2)^2} \right]. \quad (27)$$

As may be expected, η_- is real and, being proportional to q_{\parallel}^2 , introduces an anisotropy in the noise correlations. Note that every correction vanishes with q_{\parallel} so that $S_{\psi}(q_{\parallel} = 0, q_{\perp})$ suffers no modifications (at least at this lowest order). In other words, there are no changes for the structure factors perpendicular to the drive. This is a feature our model shares with the single-species DDS, leading to a discontinuity singularity at $\mathbf{q} = 0$.

When all these corrections are inserted into Eq. (20) and the ω integration performed numerically, we find that the modification to the structure factor is positive, as illustrated by the $\delta \neq 0$ curves for $S_{\psi}(q_{\parallel}, q_{\perp} = 0)$ in Fig. 10(a). Thus, we recover the DDS-like discontinuity observed in simulations (see Fig. 5): $S_{\psi}(q_{\parallel} \rightarrow 0, q_{\perp} = 0) > S_{\psi}(q_{\parallel} = 0, q_{\perp} \rightarrow 0)$. More crucially, as we examine $S_{\psi}(q_{\parallel}, q_{\perp} = 0)$ at larger q_{\parallel} , we find that the effectively $|q_{\parallel}|$ behavior in the fluctuation corrections creates a peak

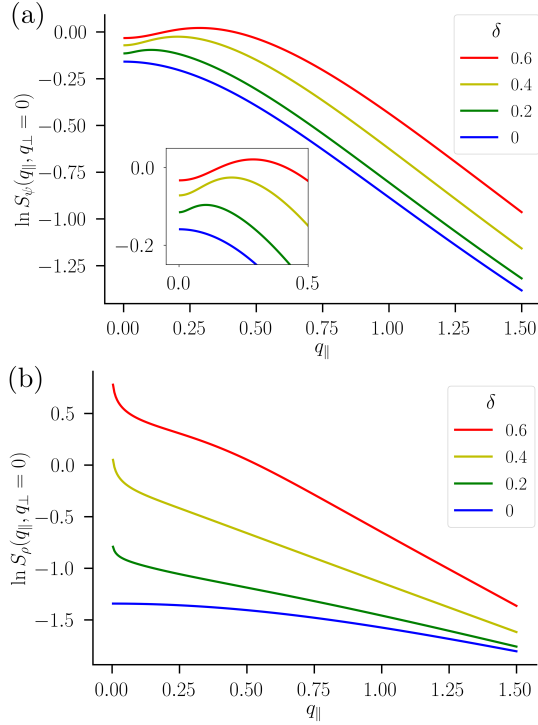


FIG. 10. Static structure factors for (a) the charge fields $S_\psi(\mathbf{q})$ and (b) the particle density $S_\rho(\mathbf{q})$ [evaluated in two dimensions along the drive direction $\mathbf{q} = (q_\parallel, q_\perp = 0)$] for different values of the drive δ and a fixed $\bar{\rho} = 0.2$, as calculated from the one loop corrections to the propagator and the noise correlations. Note the qualitative agreement between these structure factor forms and the ones found in simulations in Fig. 6(a) and Fig. 7.

at a non-trivial $q_\parallel^* > 0$. However, the theoretical result does not have a $|q_\parallel|$ -like kink at the origin, but crosses over to a smooth q_\parallel^2 . This “rounding off” is especially evident for the $\delta = 0.6$ case [inset of Fig. 10(a)]. By contrast, there is no hint of such smoothing in the data, Fig. 6(a) (although this feature may reveal itself in larger systems). Turning to the peak position, our theory finds $q_\parallel^* \approx 0.398|q_c| \approx 1.26\bar{\rho}|\delta|$. Note that it is proportional to the drive magnitude $|\delta|$ and the particle density $\bar{\rho}$. To compare this expression with data, we obtain a linear fit to the red points in Fig. 4 (2D) for small $|\delta|$ and found $q_\parallel^* \approx 0.64|\delta|$ (red line). Since the data are from a system with $\bar{\rho} = 0.5$, the theoretical value would be $q_\parallel^* \approx 0.63|\delta|$, which is in surprisingly good agreement with simulation results. Of course, this good agreement may be coincidental, as only the lowest orders in $\bar{\rho}$ and δ have been kept in the field theoretic treatment.

Finally, we consider the corrections to the static structure factors for the density fields, $S_\rho(\mathbf{q})$. Again, we defer the details of the calculation to Appendix B and present only some highlights here. The graphs for the self-energy

and noise corrections are similar to those above:

$$\Sigma_+ = \dots \circlearrowleft + \dots \circlearrowright \dots \quad (28)$$

$$\eta_+ = \dots \circlearrowright + \dots \circlearrowleft \dots \quad (29)$$

and provide us with

$$\begin{aligned} \Sigma_+ &= \int d\omega_k d\mathbf{k} \{g_0 g_- \dots + g_+^2 \dots\} \\ \eta_+ &= \int d\omega_k d\mathbf{k} \{g_+^2 \dots + g_-^2 \dots\}. \end{aligned}$$

The results are

$$\begin{aligned} \Sigma_+ &= \frac{\bar{\rho} q_\parallel^2}{16\pi} \left\{ g_0 g_- \frac{N_-}{D_-^2} \ln \left[\frac{(4\Lambda)^2 e^{-i\pi/2}}{2(v_- q_\parallel - \omega)/D_- - i|\mathbf{q}|^2} \right] \right. \\ &\quad \left. - g_+^2 \frac{N_+}{D_+^2} \ln \left[\frac{(4\Lambda)^2}{2i(v_+ q_\parallel - \omega)/D_+ + |\mathbf{q}|^2} \right] \right\} \quad (30) \end{aligned}$$

and

$$\begin{aligned} \eta_+ &= \frac{\bar{\rho}^2 q_\parallel^2}{32\pi} \sum_{\alpha=\pm} \left\{ \frac{g_\alpha^2 N_\alpha^2}{D_\alpha^3} \right. \\ &\quad \left. \times \ln \left[\frac{(4\Lambda)^4}{[2(v_\alpha q_\parallel - \omega)/D_\alpha]^2 + |\mathbf{q}|^4} \right] \right\}. \quad (31) \end{aligned}$$

It is instructive to compare these corrections to the ones for the charge fields, Σ_- and η_- . In the latter, the small ω , \mathbf{q} behavior is regulated by q_c (i.e., the velocity difference v_d). By contrast, we find logarithmic divergences in the IR regime for Σ_+ and η_+ . When inserted in Eq. (20) and the integration carried out, these generate the cusp-like structures in S_ρ as $q_\parallel \rightarrow 0$. In Fig. 10(b), we illustrate $S_\rho(q_\parallel, 0)$ for various drives. Quantitatively, there is little agreement between these S_ρ 's and the simulation values in Fig. 6(b). Nevertheless, we call attention to two important qualitative features: One is that, when driven, the fluctuations modify the small q_\parallel behavior considerably. Instead of a kink with a positive slope [downwards as $q_\parallel \rightarrow 0$, in Fig. 6(a)] for the S_ψ 's, the data here show a *cusp*³ with a large negative slope (upwards), which is especially prominent in the $\delta = 0.02$ case. This feature is certainly displayed in the theoretical S_ρ 's. Indeed, it is straightforward to uncover an IR divergence associated with the integrals regularized by $q_\parallel \neq 0$. In this case, we expect a singularity of the form of $\ln q_\parallel$ in S_ρ . To probe this property further, we plot $S_\rho(q_\parallel, 0)$ vs.

³ We have reasons (see below) to believe that S_ρ diverges as $\ln q$, so that the slope will diverge as $q \rightarrow 0$. Thus, we use the term “cusp” instead of “kink” here.

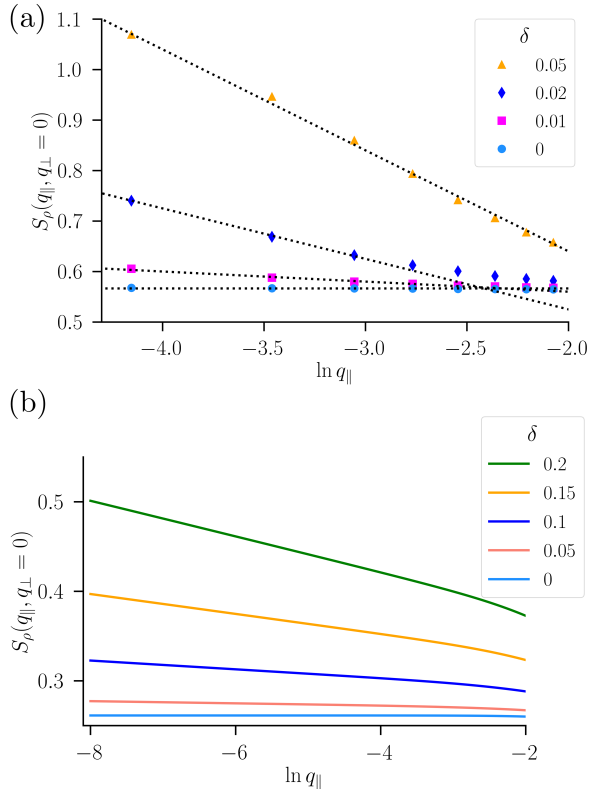


FIG. 11. Static structure factors $S_\rho(\mathbf{q})$ at small q_\parallel for simulation data in (a) [from systems with $L^2 = 400^2$ lattice sites at an average particle density of $\bar{\rho} = 0.5$, as in Fig. 7] and the field-theoretic results in (b) [obtained via numerical integration of Eq. (20) for $\bar{\rho} = 0.2$, as in Fig. 10(b)]. Note the qualitative agreement between these results: The linear behavior of S_ρ with $\ln q_\parallel$ at small $\ln q_\parallel$ values for non-zero drive $\delta > 0$ in both (a) and (b) is indicative of a logarithmic divergence, predicted by the field theory, which vanishes when $\delta = 0$, where we find a horizontal line (light blue lines and points). The straight dashed black lines in (a) are a guide to the eye to illustrate the linear behavior for small $\ln q_\parallel$.

$\ln q_\parallel$, as illustrated in Fig. 11, for both the data (a) and theoretical results (b). Surprisingly, for small q_\parallel , both display a behavior linear in $\ln q_\parallel$! We caution that such a behavior should not be extrapolated naively. It is likely that more subtle physics comes into play at larger scales *and* that higher order corrections will be important.

Note that these divergences ($\ln q_\parallel$ in $d = 2$) are reminiscent of the behavior of the single species driven diffusive system in the disordered phase. There, the static structure factors are regular in the IR limit, while the singularities appears in dynamics, as anomalous diffusion for $d \leq d_c = 2$ [49, 50]. We believe it is the presence of two different drift velocities in our model (which prevents us from studying the system in a co-moving frame) which allows the dynamic singularities to induce the ones in static quantities. It would be interesting, but beyond the scope of this paper, to find such connection and to explore how anomalous diffusion manifests in the DWRLG.

Before ending this section, note that the S_ρ 's [in Fig. 7 or 10(b)] do not display peaks like the ones in the charge S_ψ 's. Yet, as the overall density approaches the critical value and stripes form, $S_\psi(q_\parallel^*, 0)$ will diverge *and* so must $S_\rho(2q_\parallel^*, 0)$. Thus, peaks in the latter must develop. We believe that, for the values of $\bar{\rho}$ and δ shown here, such peaks are shrouded by the logarithmic divergence near the origin. Indeed, for the largest drives illustrated, there is a detectable shoulder in the theoretical S_ρ [red curve for $\delta = 0.6$ in Fig. 10(b)] and the hint of one in the data [purple curve for $\delta = 0.5$ in Fig. 7]. We see that the leading order corrections considered here reproduce the qualitative features of the structure factors for both the charge and density fields. In this sense, we believe that the approach developed here is a sound first step towards a quantitatively successful theory. The next steps would take into account the renormalization of all of the relevant couplings in Eq. (13). Although beyond the scope of the current work, pursuing a systematic analysis is a worthy goal. When completed, we are confident that the surprising properties of the DWRLG can be understood.

VI. SUMMARY AND OUTLOOK

Exploiting Monte Carlo and field-theoretic techniques, we analyzed a strongly-driven lattice gas with two species (A, B) – the Widom Rowlinson model. Restricting ourselves to systems with equal numbers of each species, there are only two control parameters: the overall particle density, $\bar{\rho}$, and the drive, δ . As the system settles into non-equilibrium steady states, many unexpected properties emerge. As both control parameters increase, the homogeneous phase gives way to phase-separation, with order stripes (slabs in 3D) *perpendicular* to the drive. The precursor of this transition appears as a “patterned” disordered phase, characterized by a non-trivial wavelength associated with the drive direction. Specifically, the static structure factor $S_\psi(q_\parallel, 0)$ (for the difference in local densities: $\psi = \rho_A - \rho_B$) has a peak at $q_\parallel^* > 0$. As $q_\parallel \rightarrow 0$ and we move away from the peak, S_ψ decreases, ending with a kink singularity (non-zero slope) at the origin. The other structure factor S_ρ (for the sum: $\rho = \rho_A + \rho_B$) displays no similar peak (far from the transition), but *increases* sharply as $q_\parallel \rightarrow 0$ so that the singularity at the origin is *cusp*-like (diverging as $\ln q_\parallel$, approximately). Following standard methods of stochastic field theory, we derived a continuum, coarse-grained description. At the Gaussian level, the *dynamic* correlation functions provide good agreement with the drift velocities of fluctuations. However, the Gaussian field theory fails to produce the novel properties of the static $S_{\rho, \psi}$. Taking into account corrections at the one-loop level (i.e., keeping the lowest non-trivial orders in $\bar{\rho}$ and δ), the field theory captures the essentials of these features (peaks in S_ψ , cusps in S_ρ). However, it compares poorly with data quantitatively.

The driven Widom Rowlinson lattice gas differs from the well-known driven Ising case in one key feature. In

the latter, the drive produces a single drifting v associated with the local density field. By contrast, due to the excluded volume interactions (between A and B), the drive in the DWRLG induces two *different* drift velocities (for ρ, ψ). The peak in S_ψ can be traced to the ratio of this velocity difference and the average diffusivity: v_d/\bar{D} . For deeper reasons we have yet to find, this aspect also appears to allow the dynamic singularities associated with anomalous diffusion [49, 50] (logarithmic in $d = 2$) to emerge in the static S_ρ . In this sense, there are many interesting directions to explore in the future, including a comprehensive analysis of the renormalization of the couplings of the theory.

We are aware of many puzzling features in this system which our simple theory cannot accommodate. The high density $\bar{\rho}$ behavior, in particular, is not accessible to the perturbative approach developed here. Interesting examples at these higher densities include the development of a peak in S_ρ for larger $\bar{\rho}$ and δ , so that $S_\rho(2q_\parallel^*, 0)$ diverges at the critical $\bar{\rho}^*$ [to accompany the divergence of $S_\psi(q_\parallel^*, 0)$], and the merging of stripes at densities above $\bar{\rho}^*$ [10] (i.e., decreasing q_\parallel^*). We are studying possible ways to improve the theoretical treatment along these lines. Clearly, it would be ideal if a full-scale renormalization group analysis can be carried out to describe the critical behavior observed in Ref. [10]. On the simulations front, improved studies with larger systems are underway so that various exponents, as well as the likely presence of anisotropic scaling, can be better measured. There is also much of interest in system at densities larger than criticality. In the previous study [10], interfaces are found to display Edwards-Wilkinson-like behavior [63]. How can such behavior be understood, as these interfaces are drifting due to the drive and *not* part of a system in thermal equilibrium? Apart from understanding how (and at what densities) configurations with N stripes can evolve into $N - 1$ stripes, we may consider the extreme high density limit. There, the system consists of just two regions with particles of A or B only (separated by thin lines of vacancies) and a handful of holes drifting through. These “drifters” interact with the interfaces, of course. Other than that, their travels through the “bulk” regions must be identical to the ordinary single-species DDS. Their interactions with the interfaces drive the latter, in a manner reminiscent of the Eden model of growing interfaces [64]. Simulation studies can be readily carried out, but our hope is that some theoretical progress is also possible in what appears to be a “minimal” system.

Beyond the particular system studied here, we should explore the vast, and likely novel, territory associated with “non-neutral” systems ($\bar{\rho}_A \neq \bar{\rho}_B$). There is also the question of whether the presence of an underlying lattice plays a crucial role. For answers, we may explore molecular dynamics simulations in a continuum, modeling colloidal particles with repulsive interactions suspended in a solvent and driven with an applied force. The hope is that connections between such computational and theoretical work can be established with physical experimen-

tal realizations.

ACKNOWLEDGMENTS

We are grateful to E. M. Horsley and Hugues Chaté for helpful discussions. Computational support was provided by the University of Tennessee and Oak Ridge National Laboratory’s Joint Institute for Computational Sciences. M.O.L. gratefully acknowledges partial funding from the Neutron Sciences Directorate (Oak Ridge National Laboratory), sponsored by the U.S. Department of Energy, Office of Basic Energy Sciences. R.D. acknowledges support from CNPq, Brazil, under grant No. 303766/2016-6.

Appendix A: Doi-Peliti formalism

The probability distribution $P(\{\sigma_{\mathbf{x}}\}, t)$ of observing particle configuration $\{\sigma_{\mathbf{x}}\}$ at time t is conveniently represented by introducing a vector $|P\rangle$ defined as

$$|P\rangle = \sum_{\{\sigma_{\mathbf{x}}\}} P(\{\sigma_{\mathbf{x}}\}, t) |\{\sigma_{\mathbf{x}}\}\rangle, \quad (\text{A1})$$

where $|\{\sigma_{\mathbf{x}}\}\rangle$ is the lattice state in the occupation number representation. Then, the master equation may be represented via a Schrödinger-like equation which reads

$$\partial_t |P\rangle = -\mathcal{L}|P\rangle, \quad (\text{A2})$$

where the Liouville operator \mathcal{L} (or pseudo-Hamiltonian) will depend on the rates given by Eq. (5). To construct the operator \mathcal{L} , we introduce creation and annihilation operators $a_{\mathbf{x}}^\dagger$ and $a_{\mathbf{x}}$, respectively. These increase or decrease by one the occupation number of the A species at site \mathbf{x} and satisfy the commutation relations $[a_{\mathbf{x}}, a_{\mathbf{y}}^\dagger] = \delta_{\mathbf{x}, \mathbf{y}}$. We also need an equivalent set $[b_{\mathbf{x}}, b_{\mathbf{y}}^\dagger] = \delta_{\mathbf{x}, \mathbf{y}}$ for the B species, both of which will commute with the A species operators. By applying the creation operators to the state $|0\rangle$ with no particles (the vacuum), we may place as many particles as we wish at any of the lattice sites \mathbf{x} . This is a problem, however, as our model is constrained by the excluded volume and particle repulsion rules, which must somehow be taken into account.

To incorporate both the excluded volume and the nearest-neighbor exclusion rule, we follow van Wijland [60] and introduce delta function operators $\delta_{\hat{n}_{\mathbf{x}}^{A,B}, m}$ (where $m = 0, 1, 2, \dots$ and $\hat{n}_{\mathbf{x}}^{A,B} = a_{\mathbf{x}}^\dagger a_{\mathbf{x}} + b_{\mathbf{x}}^\dagger b_{\mathbf{x}}$) which have the particle states $|\{\sigma_{\mathbf{x}}\}\rangle$ as eigenvectors with eigenvalues $\delta_{n_{\mathbf{x}}^{A,B}, m}$, where $n_{\mathbf{x}}^{A,B}$ is the number of A or B particles at site \mathbf{x} . It is now straightforward to write down the operator \mathcal{L} as the delta function operators can guarantee that any hopping transition that violates the excluded volume or nearest-neighbor exclusion rules will vanish. The operator reads

$$\begin{aligned}
\mathcal{L} = & \frac{1}{8\tau} \sum_{\mathbf{x}, \epsilon = \pm 1} \left\{ (1 + \epsilon\delta)(a_{\mathbf{x}-\epsilon\ell_{\parallel}}^{\dagger} - a_{\mathbf{x}}^{\dagger})a_{\mathbf{x}-\epsilon\ell_{\parallel}}\delta_{\hat{n}_{\mathbf{x}-\epsilon\ell_{\parallel}}, 1}\delta_{\hat{n}_{\mathbf{x}+\epsilon\ell_{\parallel}}, 0}\delta_{\hat{n}_{\mathbf{x}+\ell_{\perp}}, 0}\delta_{\hat{n}_{\mathbf{x}-\ell_{\perp}}, 0} \right. \\
& + (a_{\mathbf{x}-\epsilon\ell_{\perp}}^{\dagger} - a_{\mathbf{x}}^{\dagger})a_{\mathbf{x}-\epsilon\ell_{\perp}}\delta_{\hat{n}_{\mathbf{x}-\epsilon\ell_{\perp}}, 1}\delta_{\hat{n}_{\mathbf{x}+\epsilon\ell_{\perp}}, 0}\delta_{\hat{n}_{\mathbf{x}+\ell_{\parallel}}, 0}\delta_{\hat{n}_{\mathbf{x}-\ell_{\parallel}}, 0} \\
& \left. + \sum_{\bar{\epsilon} = \pm 1} (1 + \delta)(a_{\mathbf{x}-\epsilon\ell_{\parallel}-\bar{\epsilon}\ell_{\perp}}^{\dagger} - a_{\mathbf{x}}^{\dagger})a_{\mathbf{x}-\epsilon\ell_{\parallel}-\bar{\epsilon}\ell_{\perp}}\delta_{\hat{n}_{\mathbf{x}-\epsilon\ell_{\parallel}-\bar{\epsilon}\ell_{\perp}}, 1}\delta_{\hat{n}_{\mathbf{x}+\epsilon\ell_{\parallel}}, 0}\delta_{\hat{n}_{\mathbf{x}+\bar{\epsilon}\ell_{\perp}}, 0} \right\} \delta_{\hat{n}_{\mathbf{x}}, 0}\delta_{\hat{n}_{\mathbf{x}}, 0} + (a, A) \leftrightarrow (b, B), \quad (\text{A3})
\end{aligned}$$

where τ is the lattice update time step, $\ell_{\parallel} = \ell\hat{\mathbf{x}}$ is the lattice spacing in the drive direction and $\ell_{\perp} = \ell\hat{\mathbf{y}}$ is the lattice spacing in the perpendicular direction. Note that we get another set of the same terms for the B particle motion which can be generated by replacing a and A with b and B , respectively. Note that Eq. (A2) with the Liouville operator given in Eq. (A3) represents the microscopic lattice dynamics exactly. The rates $\omega_{\mathbf{x} \rightarrow \mathbf{x} + \Delta\mathbf{x}}$ in Eq. (5) are incorporated directly in Eq. (A3), where we specialize here to the square lattice for which $N_n = 8$ is the number of NN and NNN sites.

To obtain the densities within the Doi-Peliti formalism, one first introduces coherent states $|\phi_A\rangle$, which are eigenstates of the annihilation operators: $a_{\mathbf{x}}|\phi_A\rangle = \phi_{\mathbf{x}}^A|\phi_A\rangle$ (with a similar relation for species B), where $\phi_{\mathbf{x}}^A$ is a complex eigenvalue. The time evolution in Eq. (A2) can then be represented as a path integral over coherent state field configurations $\phi_{\mathbf{x}}^{A,B}$ using standard techniques [65]. The coherent states may be related to the particle densities $\rho_{\mathbf{x}}^{A,B}$ at lattice site \mathbf{x} via a Cole-Hopf transformation $[\phi_{\mathbf{x}}^{A,B}]^* = e^{\hat{\rho}_{\mathbf{x}}^{A,B}}$ and $\phi_{\mathbf{x}}^{A,B} = e^{-\hat{\rho}_{\mathbf{x}}^{A,B}} \rho_{\mathbf{x}}^{A,B}$, where $\hat{\rho}_{\mathbf{x}}^{A,B}$ is the conjugate or response field to the densities $\rho_{\mathbf{x}}^{A,B}$ at site \mathbf{x} . One then generates an action $\mathcal{J} \equiv \mathcal{J}[\hat{\rho}_{\mathbf{x}}^{A,B}, \rho_{\mathbf{x}}^{A,B}]$ that facilitates the computation of averages over stochastic trajectories of any functionals $\mathcal{O}[\rho_{\mathbf{x}}^{A,B}]$ just as in Eq. (11) in the main text. If we write the local densities as $\rho_{\mathbf{x}}^{A,B} = \bar{\rho}^{A,B} + \psi_{\mathbf{x}}^{A,B}$ at each lattice site \mathbf{x} , with $\bar{\rho}^{A,B}$ the average contribution (so that $\sum_{\mathbf{x}} \psi_{\mathbf{x}}^{A,B} = 0$), the Doi-Peliti action reads

$$\mathcal{J} = \int_0^{t_f} dt \sum_{\mathbf{x}} \left[\hat{\psi}_{\mathbf{x}}^A \partial_t \psi_{\mathbf{x}}^A + \hat{\psi}_{\mathbf{x}}^B \partial_t \psi_{\mathbf{x}}^B + \mathcal{H}_{\mathbf{x}} \right], \quad (\text{A4})$$

where $\hat{\psi}_{\mathbf{x}}^{A,B}$ are the response fields and $\mathcal{H}_{\mathbf{x}}$ is a local pseudo-Hamiltonian density that encodes the particle exclusions and hopping rates, derived from the analogous terms in the Liouville operator \mathcal{L} in Eq. (A3) by taking the expectation value of \mathcal{L} with respect to the coherent states. This development is described in standard texts, e.g., Ref. [65].

To write down the density $\mathcal{H}_{\mathbf{x}}$ explicitly for a two-dimensional lattice, it is convenient to introduce discrete derivative operators of any function $f(\mathbf{x})$ defined on the lattice sites $\mathbf{x} = (x, y)$: $\Delta_{i,j} f(\mathbf{x}) \equiv f(\mathbf{x} + i\ell_{\parallel} + j\ell_{\perp}) - f(\mathbf{x})$, where $\ell_{\perp, \parallel}$ are the lattice spacing along and perpendicular to the drive. In terms of these discrete derivative operators, we have, dropping the \mathbf{x} subscripts for notational convenience (so that $\mathcal{H} \equiv \mathcal{H}_{\mathbf{x}}$ and $\psi^{A,B} \equiv \psi_{\mathbf{x}}^{A,B}$,

etc.):

$$\begin{aligned}
\mathcal{H} = & \frac{e^{-2(\bar{\rho}^A + \psi^A) - 4(\bar{\rho}^B + \psi^B)}}{8\tau} \sum_{\epsilon = \pm 1} \left\{ (1 - e^{-\Delta_{\epsilon, 0} \hat{\psi}^A}) \right. \\
& \times (1 - \epsilon\delta)[\bar{\rho}^A + (1 + \Delta_{\epsilon, 0})\psi^A] \\
& \quad \times e^{-\Delta_{\epsilon, 0} \psi^A - (\Delta_{-\epsilon, 0} + \Delta_{0, -1} + \Delta_{0, 1})\psi^B} \\
& + (1 - e^{-\Delta_{0, \epsilon} \hat{\psi}^A})[\bar{\rho}^A + (1 + \Delta_{0, \epsilon})\psi^A] \\
& \quad \times e^{-\Delta_{0, \epsilon} \psi^A - (\Delta_{0, -\epsilon} + \Delta_{-1, 0} + \Delta_{1, 0})\psi^B} \\
& + \frac{e^{-2(\bar{\rho}^A + \psi^A) - 3(\bar{\rho}^B + \psi^B)}}{8\tau} \sum_{\epsilon_{1,2} = \pm 1} (1 - e^{-\Delta_{\epsilon_1, \epsilon_2} \hat{\psi}^A}) \\
& \times (1 - \epsilon_1 \epsilon_2 \delta)[\bar{\rho}^A + (1 + \Delta_{\epsilon_1, \epsilon_2})\psi^A] \\
& \quad \times e^{-\Delta_{\epsilon_1, \epsilon_2} \psi^A - [\Delta_{-\epsilon_1, 0} + \Delta_{0, -\epsilon_2}]\psi^B} \\
& \left. + A \leftrightarrow B, \right\} \quad (\text{A5})
\end{aligned}$$

with the last term $A \leftrightarrow B$ indicating that we need to add all the previous terms with the two particle types switched. The terms in Eq. (A5) have a certain logic: The first term (first three lines) corresponds to hops along the x -axis, while the second term (fourth and fifth lines) represents the y -axis hops. Finally, the double summation over $\epsilon_{1,2}$ (lines six through eight) represents the hops to the four NNN lattice sites. A similar formulation is straightforward for the three-dimensional case, except there are sixteen possible hopping locations.

This formulation, while derived exactly from the lattice hopping rules, is inconvenient for understanding the coarse-grained features of the system. We next need to move to a continuous description and introduce the local, coarse-grained particle densities $\rho_{A,B}(\mathbf{r})$. It will be here where the method becomes approximate, necessitating careful checks against simulation results. We begin with the Doi-Peliti action, given by Eq. (A4), with the discrete pseudo-Hamiltonian in Eq. (A5). We move to a continuous coordinate $\mathbf{x} \rightarrow \mathbf{r}$ and assume the fluctuation fields $\psi_{\mathbf{x}}^{A,B}$ are slowly varying on the scale of the lattice spacing ℓ , so we may replace them (and the corresponding response fields) with continuous fields $\psi^{A,B} \equiv \psi^{A,B}(\mathbf{r}, t)$ at any time t in the evolution. Then, the discrete derivative operators $\Delta_{i,j}$ defined above can be expanded in gradients with respect to \mathbf{r} . The expansion up to quadratic terms in ℓ is

$$\Delta_{i,j} \approx i\ell\partial_{\perp} + j\ell\partial_{\parallel} + \frac{\ell^2 i^2}{2}\partial_{\parallel}^2 + \frac{\ell^2 j^2}{2}\partial_{\perp}^2 + ij\ell^2\partial_{\parallel}\partial_{\perp}, \quad (\text{A6})$$

where i, j are the integers representing the square lattice locations $\mathbf{x} = \ell(i, j)$.

Eq. (A6) is substituted into Eqs. (A4,A5) and we expand in powers of the fields and the lattice spacing ℓ . We then perform a field redefinition and introduce the charge and density field fluctuations $\phi_{\pm} \equiv \phi_{\pm}(\mathbf{r}, t)$, which are defined via $\phi_{\pm} = \psi^A \pm \psi^B$, with corresponding response fields $\hat{\phi}_{\pm} = \hat{\psi}^A \pm \hat{\psi}^B$. Then, introducing the total particle density $\bar{\rho} = \bar{\rho}^A + \bar{\rho}^B$, we find that Eq. (A4) reduces in the continuum limit to the action given by Eq. (13) for the equal density case $\bar{\rho}_A = \bar{\rho}_B = \bar{\rho}/2$, with all of the coupling definitions stated in the main text.

Appendix B: Details of fluctuation corrections

In this appendix we give a few other details of the computation for the corrections to both the self-energy (Σ_{\pm}) and noise (η_{\pm}) terms. For $\Sigma_{-} \equiv \Sigma_{-}(\mathbf{q}, \omega)$, the two integrals, shown diagrammatically in Eq. (21), are

$$\Sigma_{-} = \int \frac{d\omega_k d\mathbf{k}}{(2\pi)^3} g_0 \left[\frac{k_{\parallel}^2}{2} + k_{\parallel} q_{\parallel} \right] \left\{ g_{-} C_{-} \left[\frac{\mathbf{q}}{2} - \mathbf{k}, \frac{\omega}{2} - \omega_k \right] G_{+} \left[\frac{\mathbf{q}}{2} + \mathbf{k}, \frac{\omega}{2} + \omega_k \right] - g_0 C_{+} \left[\frac{\mathbf{q}}{2} - \mathbf{k}, \frac{\omega}{2} - \omega_k \right] G_{-} \left[\frac{\mathbf{q}}{2} + \mathbf{k}, \frac{\omega}{2} + \omega_k \right] \right\}. \quad (\text{B1})$$

The key feature here is the mixing of the propagators for the charge and density fields [dashed and solid lines in Eq. (21)] which prevents us from eliminating the linear drift terms $v_{\pm} k_{\parallel}$ in both propagators simultaneously, unlike the case in the single-species DDS. Substituting in the expressions in Eq. (14), we evaluate the integral over ω_k first. To simplify calculations, we dropped the terms quartic in \mathbf{q} (which would have provided a UV cutoff Λ we introduce below). The result is

$$\Sigma_{-} \approx \int \frac{d\mathbf{k}}{(2\pi)^2} \frac{\bar{N} \bar{\rho} g_0 q_{\parallel}}{2\bar{D}^2 \left(\frac{|\mathbf{q}|^2}{4} + |\mathbf{k}|^2 \right) - i\bar{D} \left[\omega - \bar{v} q_{\parallel} + v_d k_{\parallel} \right]} \left[g_{-} \left(\frac{q_{\parallel}}{2} - k_{\parallel} \right) - g_0 \left(\frac{q_{\parallel}}{2} + k_{\parallel} \right) \right] \quad (\text{B2})$$

to leading order in the average density $\bar{\rho}$. After integrating k_{\perp} on the real line first, the remaining $\int k_{\parallel}$ is naïvely linearly divergent. However, by imposing the UV cutoff $\Lambda = \pi/\ell$, we find the result in the main text:

$$\Sigma_{-} \approx \frac{\bar{\rho} g_0 \bar{N} v_d q_{\parallel}}{32\pi \bar{D}^3} \left\{ \left[\frac{q_{\parallel}}{q_c} (g_{-} - g_0) - i(g_{-} + g_0) \right] \times \ln \left[\frac{16\Lambda^2}{2i(\bar{v} q_{\parallel} - \omega)/\bar{D} + q_c^2 + |\mathbf{q}|^2} \right] + i(g_{-} + g_0) \right\}. \quad (\text{B3})$$

Here, $\bar{D} = (D_{+} + D_{-})/2$ is the average diffusivity, $\bar{v} = (v_{+} + v_{-})/2$ the average velocity, $v_d = -\bar{\rho} \delta v$ the velocity difference, $q_c = v_d/2\bar{D}$ the crossover wavenumber,

and $\bar{N} = (N_{-} + N_{+})/2$ is the noise correlation magnitude. The real part, $\text{Re} \Sigma_{-}$, is given in Section V. For completeness, we provide the imaginary part here:

$$\text{Im} \Sigma_{-} = \frac{\bar{\rho} g_0 \bar{N} q_{\parallel}}{16\pi \bar{D}^2} \left\{ (g_0 - g_{-}) q_{\parallel} \tan^{-1} \left[\frac{2(\bar{v} q_{\parallel} - \omega)}{\bar{D}(q_c^2 + |\mathbf{q}|^2)} \right] - \frac{(g_0 + g_{-}) q_c}{2} \ln \left[\frac{2^{12} \bar{D}^2 \Lambda^4 e^{-4}}{[\bar{v} q_{\parallel} - \omega]^2 + 16\bar{D}^2 [q_c^2 + |\mathbf{q}|^2]^2} \right] \right\}. \quad (\text{B4})$$

Meanwhile, the single integral associated with the noise correction for the charge field is

$$\eta_{-} \approx \frac{[\bar{N} \bar{\rho} g_0 q_{\parallel}]^2}{\bar{D}} \int \frac{d\mathbf{k}}{(2\pi)^2} \frac{|\mathbf{q}|^2 + 4|\mathbf{k}|^2}{[\omega - \bar{v} q_{\parallel} - v_d k_{\parallel}]^2 + \left[\frac{\bar{D} |\mathbf{q}|^2}{2} + 2\bar{D} |\mathbf{k}|^2 \right]^2} \quad (\text{B5})$$

Similarly, after the ω_k integration, we find the self-energy for the density field, represented by Eq. (28), to be

$$\Sigma_{+} \approx \frac{\bar{\rho} q_{\parallel}^2}{2} \int \frac{d\mathbf{k}}{(2\pi)^2} \left\{ \frac{N_{-} g_0 g_{-}}{2D_{-}^2 \left[\frac{|\mathbf{q}|^2}{4} + |\mathbf{k}|^2 \right] - iD_{-} (\omega - v_{-} q_{\parallel})} - \frac{N_{+} g_{+}^2}{2D_{+}^2 \left[\frac{|\mathbf{q}|^2}{4} + |\mathbf{k}|^2 \right] - iD_{+} (\omega - v_{+} q_{\parallel})} \right\}, \quad (\text{B6})$$

leading to the result in Eq. (30). For completeness, we display its real and imaginary parts:

$$\text{Re} \Sigma_{+} \approx \frac{\bar{\rho} q_{\parallel}^2}{32\pi} \left\{ \frac{N_{-} g_0 g_{-}}{D_{-}^2} \ln \left[\frac{256\Lambda^4}{\left[\frac{2}{D_{-}} (v_{-} q_{\parallel} - \omega) \right]^2 + |\mathbf{q}|^4} \right] - \frac{N_{+} g_{+}^2}{D_{+}^2} \ln \left[\frac{256\Lambda^4}{\left[\frac{2}{D_{+}} (v_{+} q_{\parallel} - \omega) \right]^2 + |\mathbf{q}|^4} \right] \right\}. \quad (\text{B7})$$

and

$$\text{Im} \Sigma_{+} \approx \frac{\bar{\rho} q_{\parallel}^2}{16\pi} \left\{ \frac{N_{+} g_{+}^2}{D_{+}^2} \tan^{-1} \left[\frac{2(v_{+} q_{\parallel} - \omega)}{D_{+} |\mathbf{q}|^2} \right] - \frac{N_{-} g_0 g_{-}}{D_{-}^2} \tan^{-1} \left[\frac{2(v_{-} q_{\parallel} - \omega)}{D_{-} |\mathbf{q}|^2} \right] \right\}. \quad (\text{B8})$$

Finally, the correction to the noise correlations, $\bar{N}_{+} = N_{+} \bar{\rho} |\mathbf{q}|^2 + \eta_{+}$ [associated with Eq. (29)] is given by

$$\eta_{+} \approx \frac{\bar{\rho}^2 q_{\parallel}^2}{4} \int \frac{d\mathbf{k}}{(2\pi)^2} \left\{ \sum_{\alpha=\pm} \frac{g_{\alpha}^2 N_{\alpha}^2 \left[\frac{|\mathbf{q}|^2}{4} + |\mathbf{k}|^2 \right]}{(\omega - v_{\alpha} k_{\parallel})^2 \frac{D_{\alpha}}{4} + D_{\alpha}^3 \left[\frac{|\mathbf{q}|^2}{4} + |\mathbf{k}|^2 \right]^2} \right\}, \quad (\text{B9})$$

which leads to the result in Eq. (31).

-
- [1] S. A. Brazovskii and S. G. Dmitriev, Zh. Eksp. Teor. Fiz. **69**, 979 (1975), [Sov. Phys. JETP **42**, 497-502 (1976)].
- [2] M. Seul and D. Andelman, Science **267**, 476 (1995).
- [3] J. Li, I. S. Aranson, W.-K. Kwok, and L. S. Tsimring, Phys. Rev. Lett. **90**, 134301 (2003).
- [4] J. B. Swift and P. C. Hohenberg, Phys. Rev. A **15**, 319 (1977).
- [5] M. C. Cross and P. C. Hohenberg, Rev. Mod. Phys. **65**, 851 (1993).
- [6] M. Teubner and R. Strey, J. Chem. Phys. **87**, 3195 (1987).
- [7] S. Leibler and D. Andelman, J. Phys. France **48**, 2013 (1987).
- [8] S. A. Brazovskii, Zh. Eksp. Teor. Fiz. **68**, 175 (1975), [Sov. Phys. JETP **41**, 85-89 (1975)].
- [9] S. A. Brazovskii, I. E. Dzyaloshinskii, and A. R. Muratov, Zh. Eksp. Teor. Fiz. **93**, 1110 (1987), [Sov. Phys. JETP **66**, 625-633 (1987)].
- [10] R. Dickman and R. K. P. Zia, Phys. Rev. E **97**, 062126 (2018).
- [11] P. Sánchez, M. R. Swift, and P. J. King, Phys. Rev. Lett. **93**, 184302 (2004).
- [12] Y. Zhu and Y. Ma, J. Chem. Phys. **118**, 9023 (2003).
- [13] C. Du, K. R. Sütterlin, A. V. Ivlev, H. M. Thomas, and G. E. Morfill, EPL **99**, 45001 (2012).
- [14] S. Patra, D. Das, R. Rajesh, and M. K. Mitra, Phys. Rev. E **97**, 022108 (2018).
- [15] A. K. Chatterjee, B. Daga, and P. K. Mohanty, Phys. Rev. E **94**, 012121 (2016).
- [16] E. Ising, Z. Phys. **31**, 253 (1925).
- [17] M. Blume, V. J. Emery, and R. B. Griffiths, Phys. Rev. A **4**, 1071 (1971).
- [18] R. Potts, Math. Proc. Camb. Philos. Soc. **48**, 106 (1952).
- [19] R. Fowler, Math. Proc. Camb. Philos. Soc. **32**, 144 (1936).
- [20] J. R. Lacher, Proc. Roy. Soc. **A161**, 525 (1937).
- [21] T. D. Lee and C. N. Yang, Phys. Rev. **87**, 410 (1952).
- [22] H. V. N. Temperley, Proc. Phys. Soc. **A67**, 233 (1954).
- [23] J. Bernasconi and F. Rys, Phys. Rev. B **4**, 3045 (1971).
- [24] J. Lajzerowicz and J. Sivardière, Phys. Rev. A **11**, 2079 (1975).
- [25] S. Katz, J. L. Lebowitz, and H. Spohn, J. Stat. Phys. **34**, 497 (1984).
- [26] S. Katz, J. L. Lebowitz, and H. Spohn, Phys. Rev. B **28**, 1655(R) (1983).
- [27] K. t. Leung, B. Schmittmann, and R. K. P. Zia, Phys. Rev. Lett. **62**, 1772 (1989).
- [28] P. L. Garrido, J. L. Lebowitz, C. Maes, and H. Spohn, Phys. Rev. A **42**, 1954 (1990).
- [29] Z. Cheng, P. L. Garrido, J. L. Lebowitz, and J. L. Vallés, Europhysics Letters (EPL) **14**, 507 (1991).
- [30] B. Schmittmann and R. K. P. Zia, Phys. Rev. Lett. **66**, 357 (1991).
- [31] J. L. Vallés, K. t. Leung, and R. K. P. Zia, Journal of Statistical Physics **56**, 43 (1989).
- [32] D. H. Boal, B. Schmittmann, and R. K. P. Zia, Phys. Rev. A **43**, 5214 (1991).
- [33] B. Schmittmann, K. Hwang, and R. K. P. Zia, Europhysics Letters (EPL) **19**, 19 (1992).
- [34] K. E. Bassler, B. Schmittmann, and R. K. P. Zia, Europhysics Letters (EPL) **24**, 115 (1993).
- [35] K. t. Leung and R. K. P. Zia, Phys. Rev. E **56**, 308 (1997).
- [36] D. Krenzel, S. Strobl, A. Sack, M. Heckel, and T. Pöschel, Granular Matter **15**, 377 (2013).
- [37] A. Wysocki and H. Löwen, Phys. Rev. E **79**, 041408 (2009).
- [38] M. P. Ciamarra, A. Coniglio, and M. Nicodemi, Phys. Rev. Lett. **94**, 188001 (2005).
- [39] M. P. Ciamarra, A. Sarracino, M. Nicodemi, and A. Coniglio, in *Traffic and Granular Flow '05*, edited by A. Schadschneider, T. Pöschel, R. Kühne, M. Schreckenberg, and D. E. Wolf (2007), pp. 41–51.
- [40] R. Dickman and G. Stell, J. Chem. Phys. **102**, 8674 (1995).
- [41] F. Spitzer, Adv. Math. **5**, 246 (1970).
- [42] T. E. Harris, J. Appl. Prob. **2**, 323 (1965).
- [43] T. M. Liggett, *Interacting Particle Systems* (Springer-Verlag, New-York, 1985), 1st ed.
- [44] H. Spohn, *Large Scale Dynamics of Interacting Particles* (Springer Verlag, Heidelberg, 1991).
- [45] T. M. Liggett, *Stochastic Interacting Systems: Contact, Voter, and Exclusion Processes* (Springer Verlag, Berlin, 1999).
- [46] T. Chou, K. Mallick, and R. K. P. Zia, Rep. Prog. Phys. **74**, 116601 (2011).
- [47] B. Widom and J. S. Rowlinson, J. Chem. Phys. **52**, 1670 (1970).
- [48] P. C. Hohenberg and B. I. Halperin, Rev. Mod. Phys. **49**, 435 (1977).
- [49] H. van Beijeren, R. Kutner, and H. Spohn, Phys. Rev. Lett. **54**, 2026 (1985).
- [50] H. K. Janssen and B. Schmittmann, Z. Phys. B: Condens. Matter **63**, 517 (1986).
- [51] B. Schmittmann and R. K. P. Zia, *Statistical mechanics of driven diffusive systems* (Academic Press, San Diego, 1995).
- [52] H. K. Janssen and B. Schmittmann, Z. Phys. B **64**, 503 (1986).
- [53] K. t. Leung and J. L. Cardy, J. Stat. Phys. **44**, 576 (1986).
- [54] P. C. Martin, E. D. Siggia, and H. A. Rose, Phys. Rev. A **8**, 423 (1973).
- [55] H.-K. Janssen, Z. Physik B **23**, 377 (1976).
- [56] C. de Dominicis, J. Phys. Colloq. **37**, 247 (1976).
- [57] A. Lefèvre and G. Biroli, J. Stat. Mech. **2007**, P07024 (2007).
- [58] M. Doi, J. Phys. A: Math. Gen. **9**, 1465 (1976).
- [59] L. Peliti, J. Physique **46**, 1469 (1985).
- [60] F. van Wijland, Phys. Rev. E **63**, 022101 (2001).
- [61] R. Dickman and R. Vidigal, Braz. J. Phys. **33**, 73 (2003).
- [62] D. Das, A. Basu, M. Barma, and S. Ramaswamy, Phys. Rev. E **64**, 021402 (2001).
- [63] S. F. Edwards and D. R. Wilkinson, Proc. R. Soc. A **381**, 17 (1982).
- [64] M. Eden, in *Proc. Fourth Berkeley Symp. on Mathematical Statistics and Probability*, edited by J. Neyman (1961), vol. 4, pp. 223–239.
- [65] U. C. Täuber, *Critical Dynamics* (Cambridge University Press, Cambridge, 2014).